minerals

MDPI

Article

Geochronology of the Baishi W-Cu Deposit in Jiangxi Province and Its Geological Significance

Li Li [1,2], Hai-Li Li [3,4,*], Guo-Guang Wang [2,*] and Jian-Dong Sun [3]

[1] School of Civil Engineering, Jiangsu Urban and Rural Construction College, Changzhou 213147, China
[2] State Key Laboratory for Mineral Deposits Research, Institute of Geo-Fluids, School of Earth Sciences and Engineering, Nanjing University, Nanjing 210023, China
[3] Nanjing Center, China Geological Survey, Nanjing 210016, China
[4] CAS Key Laboratory of Crust-Mantle Materials and Environments, School of Earth and Space Sciences, University of Science and Technology of China, Hefei 230026, China
* Correspondence: lhaili@mail.ustc.edu.cn (H.-L.L.); ggwang@nju.edu.cn (G.-G.W.)

Abstract: The Baishi W-Cu deposit is located in the Nanling metallogenic belt, which is famous for its numerous W deposits and reserves. The formation age of this deposit remains unclear. In order to further infer the formation age of the deposit, this study conducted detailed LA-ICP-MS U-Pb isotopic analyses of zircon and monazite selected from ore-related Baishi granite. The LA-ICP-MS zircon U-Pb weighted average ages of Baishi granite were determined to be 223 $\pm$ 2 Ma and 226 $\pm$ 1 Ma, and the LA-ICP-MS U-Pb weighted average ages of monazite were determined to be 224 $\pm$ 2 Ma and 223 $\pm$ 1 Ma. The BSE image of monazite was homogeneous, and the pattern of rare earth elements had an obvious negative Eu anomaly, indicating that monazite was of magmatic origin. Combining the ages of zircon and monazite, this study inferred that Baishi granite and the Baishi W-Cu deposit formed in the Triassic. The determination of the ore-forming event of the Baishi W-Cu deposit provides new data regarding the important Indosinian (Triassic) mineralization events in the Nanling metallogenic belt and suggests that geologists should strengthen the prospecting work of Indosinian tungsten deposits in the Nanling area. In terms of tectonic setting, it was inferred that the Triassic Baishi W-Cu deposit was formed in the extensional environment after intracontinental orogeny.

Keywords: Nanling region; Baishi; zircon U-Pb; monazite U-Pb; Indosinian

Citation: Li, L.; Li, H.-L.; Wang, G.-G.; Sun, J.-D. Geochronology of the Baishi W-Cu Deposit in Jiangxi Province and Its Geological Significance. *Minerals* **2022**, *12*, 1387. https://doi.org/10.3390/min12111387

Academic Editor: Maria Boni

Received: 12 September 2022
Accepted: 28 October 2022
Published: 30 October 2022

1. Introduction

China has the richest tungsten resources in the world, and most of the tungsten deposits are concentrated in South China. Among them, the Nanling metallogenic belt is the most famous tungsten polymetallic metallogenic belt, and the study of tungsten polymetallic mineralization related to Mesozoic granites is a hot topic for geologists [1–4]. The Yanshanian (Jurassic–early Cretaceous) is considered as the most important stage of large-scale felsic magmatism and mineralization in the Nanling region [5–11]. Recently, with the expansion of the research scope and the progress of research techniques and methods, Indosinian granites and related W mineralization in the Nanling metallogenic belt, and even in the whole of South China, have been reported in an increasing number of papers [12–17]. Indosinian metallogenic events are considered to have good metallogenic potential, and the prospecting work carried out on Indosinian deposits should be strengthened [18–22].

Among the isotope dating methods, U-Th-Pb isotope chronology is the most widely used; it can predict the exact time of the generation of geological bodies and events and is an important means to study geological evolution. Zircon is a common mineral used for U-Th-Pb isotope dating, as it is extremely stable. It is the most widely used mineral for U-Pb dating for its high contents of U and Th, low contents of common Pb, and particularly high closure temperature [23].

Monazite ((Ce,La,Th)PO_4) is a phosphate mineral rich in LREEs. It is commonly found as an accessory mineral in peraluminous granites and Ca-poor metamorphic rocks [24] and sometimes forms in sedimentary rocks [25]. In recent years, it has become one of the more important dating minerals, because it contains a large amount of the highly radioactive elements of Th and U and very little common Pb [26–29].

The Baishi W-Cu deposit is located in the Xingguo–Ningdu ore concentration area of Jiangxi Province, and its metallogenic chronology and geodynamic setting are still unclear. Baishi granite is ore-forming rock, as it is ore bearing and has a close relationship with the ore veins. To clearly determine the forming ages of Baishi granite and of the Baishi W-Cu deposit, this study conducted LA-ICP-MS U-Pb dating using both zircon and monazite. This study summarized the metallogenic epoch of tungsten polymetallic deposits in the Nanling metallogenic belt and confirmed the important role of Indosinian mineralization in the Nanling region.

2. Geological Setting

The study area is located at the intersection of the eastern end of the EW tectonic-magmatic zone of Nanling and the Yushan depression zone of the western uplift zone of Wuyi Mountain (Figure 1A). In terms of metallogenic melt, the study area belongs to the eastern part of the Nanling metallogenic belt and is part of the Xingguo–Ningdu ore cluster (Figure 1B).

The oldest rocks in the study area are the Sinian (Edicaran) shallow marine facies strata that underwent lower greenschist-facies metamorphism. The lithologic assemblage is represented by metatuffs, metasandstones, phyllites, and siliceous rocks. Cambrian formation is represented by rhythmic sandstone-slate formation. Devonian and Carboniferous formations occur only sporadically; the former is mainly composed of continental clastic rocks with a few marine calc-argillaceous rocks, and the latter is represented by mud–sand detrital deposits in transition from continental to marine facies. A few outcrops are referred to have formed during the Permian–Jurassic interval. Permian formation is concerned with conglomerates, siltstones, sandstones, and tuffs. Jurassic formation contains calcareous shales and limestones. Cretaceous volcanic rocks, red sandstones, and conglomerates are widespread (Figure 1C).

There are mainly two NE-trending regional deep faults in the study area, namely, the Wan'an fault in the northwest and the Shefu fault in the southeast (Figure 1C). The fold deformation in the region is intense, and the fold hinges are mainly in the direction of nearly N-S or NW trending.

Magmatic rocks in the study area are well developed, and magmatic activities last for a long time, showing the characteristics of Caledonian (Silurian–Devonian), Indosinian, and Yanshanian multi-stage activities. The lithology is mainly acidic granites, showing a close relationship with tungsten, tin, molybdenum, copper, and other polymetallic mineralization (Figure 1C).

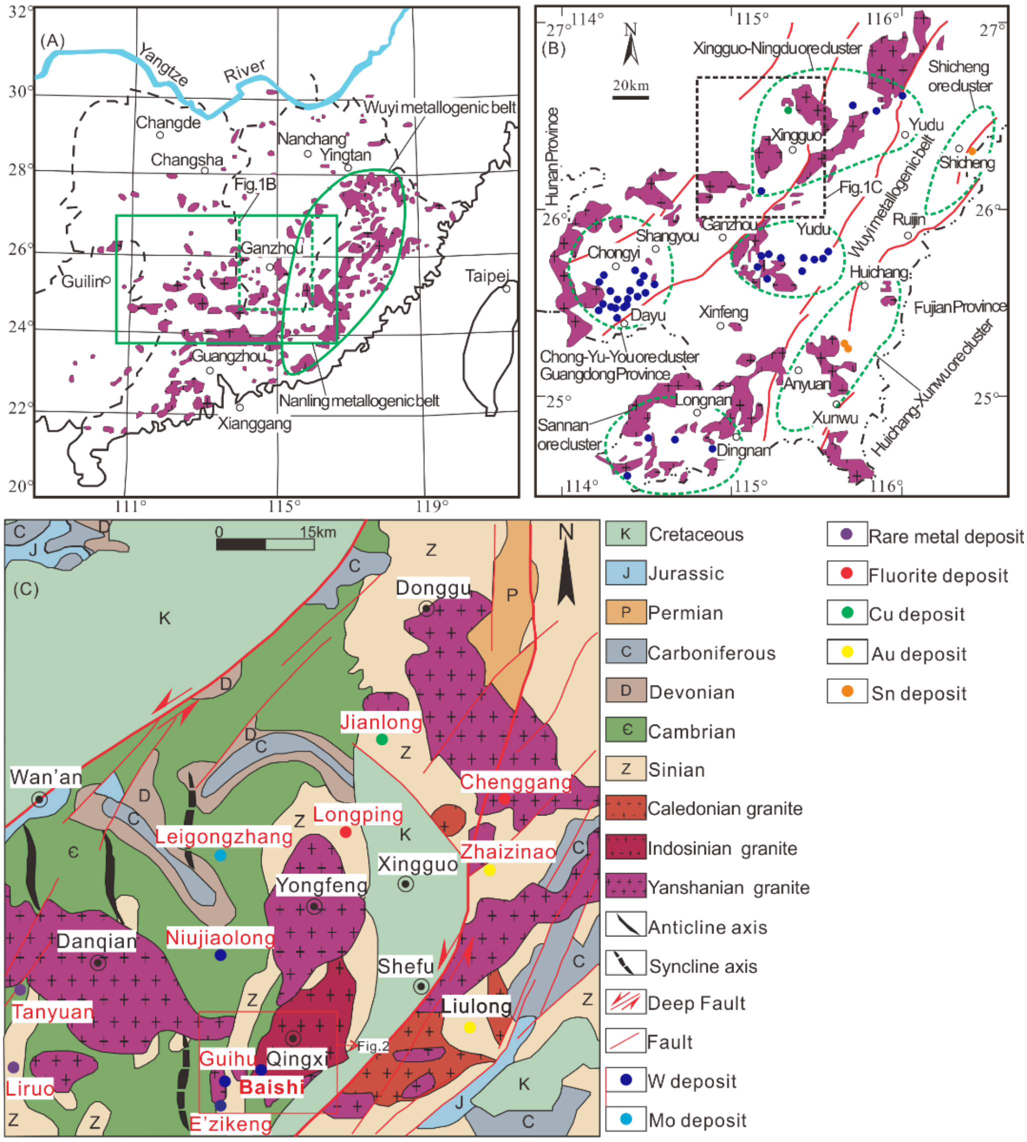

Figure 1. (**A**) Simplified map showing the distribution of Yanshanian granites in South China (modified from [30]). (**B**) Schematic distribution map of tungsten ore cluster and typical W-Sn deposits in South Jiangxi Province (modified from [18]). (**C**) Regional geological map of Baishi W-Cu deposit (modified from [31]).

3. Petrology

Baishi granite, as the main igneous rock in this W-Cu deposit, occurs as grayish-white-to-grayish-yellow intermediate granite felsic stock (Figure 2A,B). The essential minerals of granite are plagioclase, K-feldspar, quartz, muscovite, and biotite (Figure 2C,D). The accessory minerals contain apatite, rutile, zircon, and monazite. Alterations are widespread, appearing in the form of reactions such as carbonatation and chloritization. Granite shows close spatial and genetic relations with W-Cu mineralization, including the following aspects: (1) Baishi granite contains ore vein and disseminated mineralization, as we could see in the field images (Figure 2A,B) and microphotographs (Figure 2E,F). (2) The average content of W in the three samples of Baishi granite was 38.17 ppm (unpublished data from Nanjing Center, China Geological Survey), which was much higher than the average contents of the continental crust (1.0 ppm), upper crust (1.4 ppm), and lower crust (0.6 ppm) [32]. Thus, Baishi granite and related ore bodies were considered to have formed simultaneously.

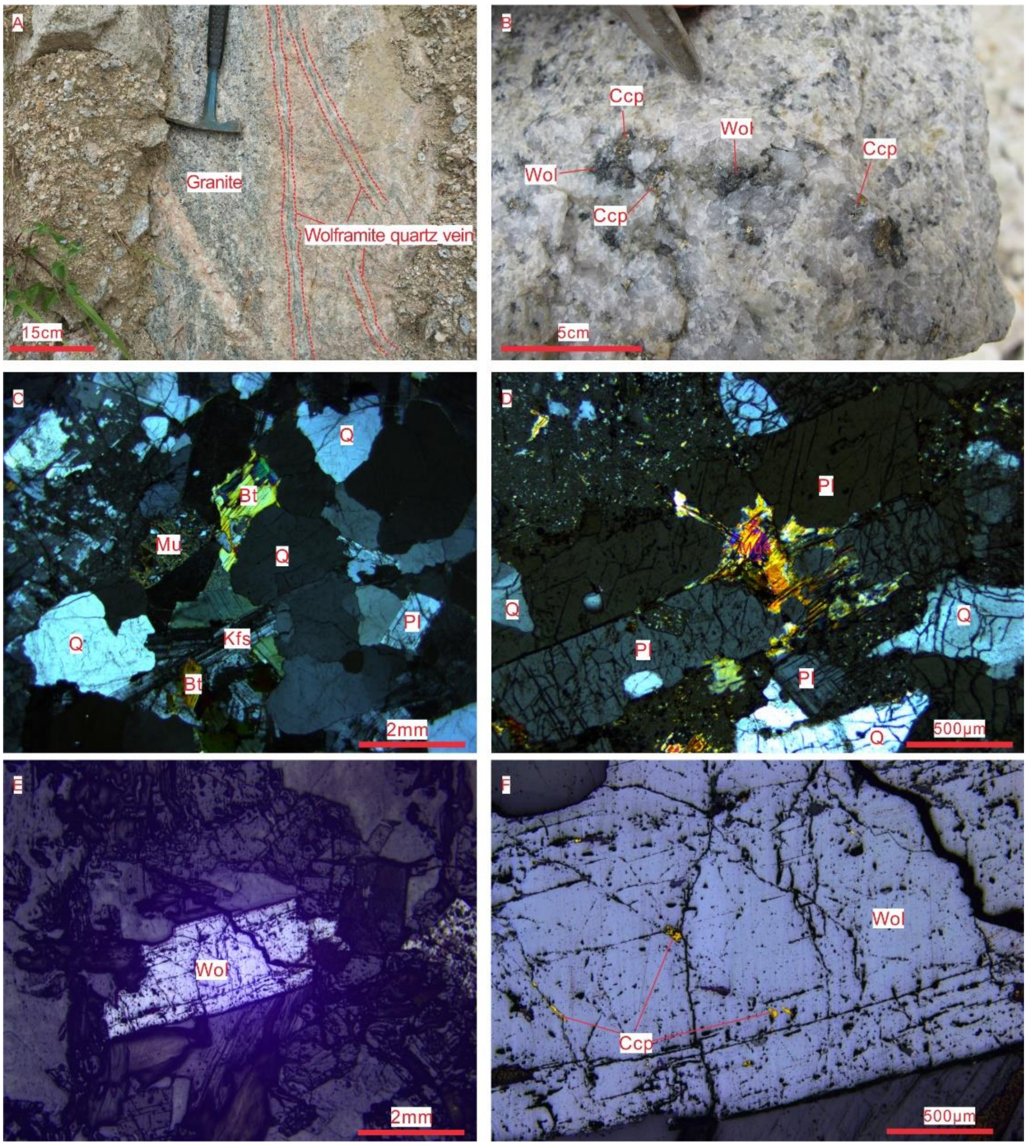

Figure 2. Photographs of Baishi granite. (**A**) Field photo of Baishi granite that contained wolframite quartz veins. (**B**) Hand specimen picture of Baishi granite that contained disseminated wolframite and chalcopyrite. (**C**,**D**) Cross-polarized light microphotographs of Baishi granite. (**E**,**F**) Reflected light microphotographs of Baishi granite that contained wolframite and chalcopyrite. Abbreviations: Wol, wolframite; Ccp, chalcopyrite; Q, quartz; Kfs, k-feldspar; Pl, plagioclase; Bt, biotite; Mu, muscovite.

4. Ore Deposit Geology

The Baishi W-Cu deposit had been exploited since the founding of the People's Republic of China. After that, exploration team No. 220 (now called Jiangxi Geological Survey and Exploration Institute), Gannan Brigade, and other units carried out general surveys and explored the Baishi W-Cu deposit until 1958. The Baishi W-Cu deposit is a medium-sized tungsten polymetallic deposit with Cu, Mo, Bi, and Zn.

The exposed strata of the mining area are lower Cambrian strata, composed of slate intercalated with sandstone and phyllite, and the stratigraphic trend is nearly north–south. The mining area is generally controlled by the north–south structure (Figure 3). The veins are filled in the fissures of WNW and NNE. The fissures of this group are mainly in the WNW direction, which have obvious tensile characteristics. However, the veins of the NEE fissures are small and dense, and belong to compressional and torsional fractures according to their mechanical properties. A massive ore body is found at the intersection of two groups of fractures in the WNW and the NNE fissures.

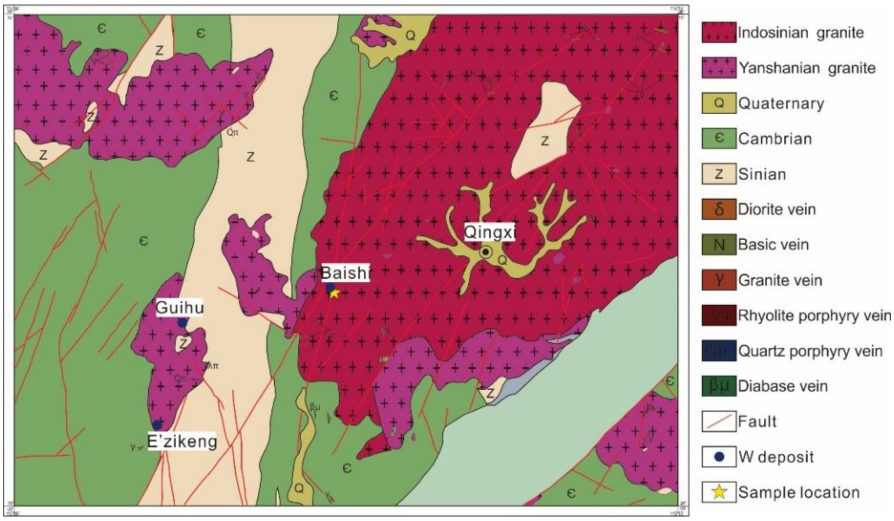

Figure 3. Geological deposit map of Baishi W-Cu deposit region (modified from [33]).

The formation of the Baishi W-Cu deposit is closely related to Baishi granite (Figure 2A,B). Granite and adjacent smaller intrusions with nodules are exposed in the mining area. The alterations closely related to mineralization include silication, sericitization, muscovitization, chloritization, and greisenization (Figure 2A,B).

This deposit belongs to a wolframite–chalcopyrite quartz vein type. The tungsten-bearing vein ore bodies are mainly in the WNW formation and occur secondarily in the NNE formation. In general, the veins are irregular, and the local variations are great. Along the vertical and horizontal directions, the pinching side appears and reappears. The main mineral in the ore vein is wolframite. A variety of sulfide minerals are associated, especially chalcopyrite (Figure 2E,F). Metal minerals include wolframite, chalcopyrite, marmatite, molybdenite, bismuth, and scheelite.

The mineralization in this mining area can be divided into the following stages: (1) The quartz–wolframite stage. This stage belongs to the pegmatic vaporization stage. The minerals generated are quartz, wolframite, molybdenite, muscovite, beryl, topaz, etc. In this stage, the metal and vapor-forming minerals are more common on both sides of the veins. There is an abundance of wolframite deposits in this stage. (2) The quartz sulfide stage. This stage is roughly in the middle-temperature stage. A large amount of chalcopyrite precipitate can be found in this period. Fluorite, sericite, and other minerals form in this stage. (3) The carbonate stage. This stage is a low-temperature hydrothermal stage in which calcite, sericite, and low-temperature silica dominate.

5. Sampling and Analytical Methods

Two samples were studied in this research study, and they are collected in the Baishi W-Cu deposit (Figure 3). One sample was chosen for obtaining the phase and compositional map using TESCAN Intergrated Mineral Analyzer (TIMA). The TIMA results were analyzed at Nanjing Hongchuang Geological Exploration Technology Service Co., Ltd. TIMA is a Mira-3 scanning electroscope equipped with four energy-dispersive X-ray spectroscopy devices (EDS; EDAX Element 30). For the experiment, we used an acceleration voltage of 25 kV and a probe current of 9 nA. The working distance was set to 15 mm. The pixel spacing was set to 3 μm, and the dot spacing was set to 9 μm. The sample was scanned using the liberation analysis module. The method is described in detail in [34].

Zircon grains for LA-ICP-MS U-Pb dating and monazite grains for LA-ICP-MS U-Pb dating and rare earth elements analyses were separated from Baishi granite using conventional heavy-liquid and magnetic separation methods. Representative zircon and monazite grains were hand-picked under a binocular microscope, mounted on an epoxy resin disk, and polished down to nearly half the section to expose their internal structures for LA-

ICP-MS analyses. Zircon and monazite were documented with transmitted and reflected light micrographs as well as with cathodoluminescence (CL) images and back-scattered electron (BSE) images, respectively, to reveal their internal structures, and the mount was vacuum-coated with carbon. The CL and BSE images were taken with a scanning electron microscope at State Key Laboratory for Mineral Deposit Research (MiDeR), Nanjing University. U-Pb dating and rare earth elements were analyzed using LA-ICP-MS at Wuhan SampleSolution Analytical Technology Co., Ltd., Wuhan. Laser sampling was performed using an excimer laser ablation system (GeoLas Pro). An Agilent 7900 ICP-MS instrument was used to acquire ion-signal intensities. Helium was used as a carrier gas. Argon was used as the make-up gas and mixed with the carrier gas via a T-connector before entering the ICP. To decrease the detection limit and improve precision at spot sizes of 30 μm for zircon and 16 μm for monazite, nitrogen was added to the central gas flow (Ar + He) of the Ar plasma. The 91,500 and GJ-1 standard zircons were analyzed to correct isotopic fractionation and for zircon grains. The GJ-1 standard zircon analysis yielded an age of 604.2 ± 2.6 Ma (2σ, n = 8). The 44,069 and NIST 610 standards were used as external standards for monazite U-Pb dating and rare earth element calibration, respectively. The off-line selection and integration of background and quantitative calibration for rare earth element analyses and U-Pb dating were performed using in-house software ICPMSDataCal. Common Pb correction and the determination of the ages of the samples were carried out according to the method proposed by [35]. Data processing was carried out using the Isoplot programs of [36].

6. Results

6.1. TIMA Mineral Map

A section of Baishi granite was used to create the TIMA mineral map. The results are shown in Figure 4. The phase map was described using the backscattered electron (BSE) image and EDS data. Additionally, the percentage of minerals was calculated as the modal volume property. The potential reasons for unclassified minerals are as follows: (1) the energy spectra among different minerals are too close for the machine to identify, and (2) the grain size of the mineral is less than 3 μm, which is the pixel space. We could see that Baishi granite contained amounts of quartz (46.36%), albite (23.82%), and K-feldspar (10.28%). Muscovite (9.46%) and chlorite (3.56%) were ubiquitous. Most of the biotite was altered, and only little was reserved (0.59%). Baishi granite contained lots of accessory minerals, such as tourmaline (0.31%), apatite (0.25%), rutile (0.08%), zircon (0.02%), and monazite (0.01%). There were also some late carbonate minerals (0.15%) and clay minerals (0.02%).

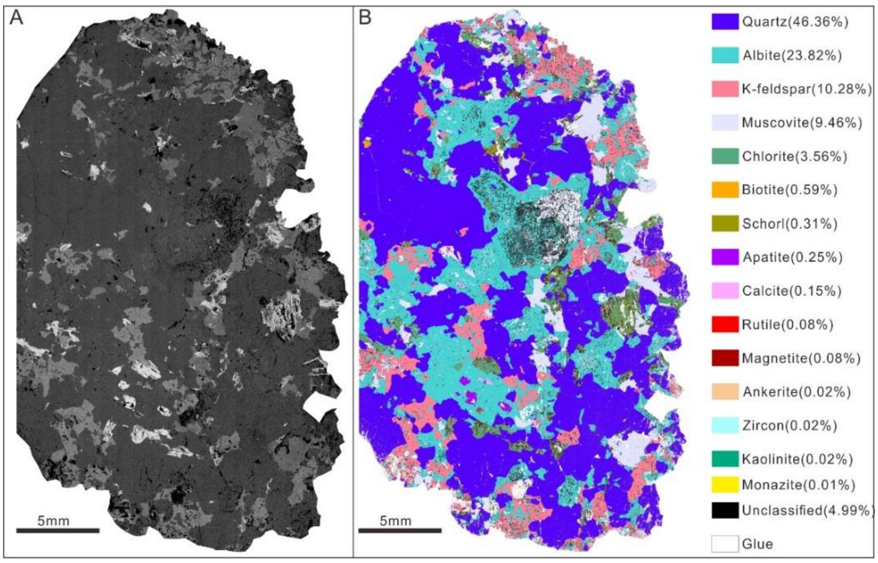

Figure 4. (**A**) BSE photo of Baishi granite. (**B**) Phase map and composition of Baishi granite.

6.2. LA-ICP-MS Zircon U-Pb Dating

The LA-ICP-MS analyses using zircon U-Pb isotopes were conducted on two granite samples. The results are summarized in Table 1. CL images of the representative zircon grains with $^{206}Pb/^{238}U$ ages are shown in Figure 5. The zircons were generally euhedral, short-to-long prismatic, colorless, and transparent. The crystal length ranged from 150 to 500 µm, with length-to-width ratios of 1:1 to 4:1. Most of the zircons showed clear oscillatory zoning in the CL images (Figure 5A,C), as is the case of magmatic zircon. The zircons showed variable U (151–2241 ppm) and Th (94–805 ppm) concentrations, with Th/U ratios ranging from 0.07 to 0.86 (Table 1). The Th/U ratios were consistent with the general magmatic zircons but were mostly higher than metamorphic zircons, which normally show lower Th/U ratios (<0.1) [37].

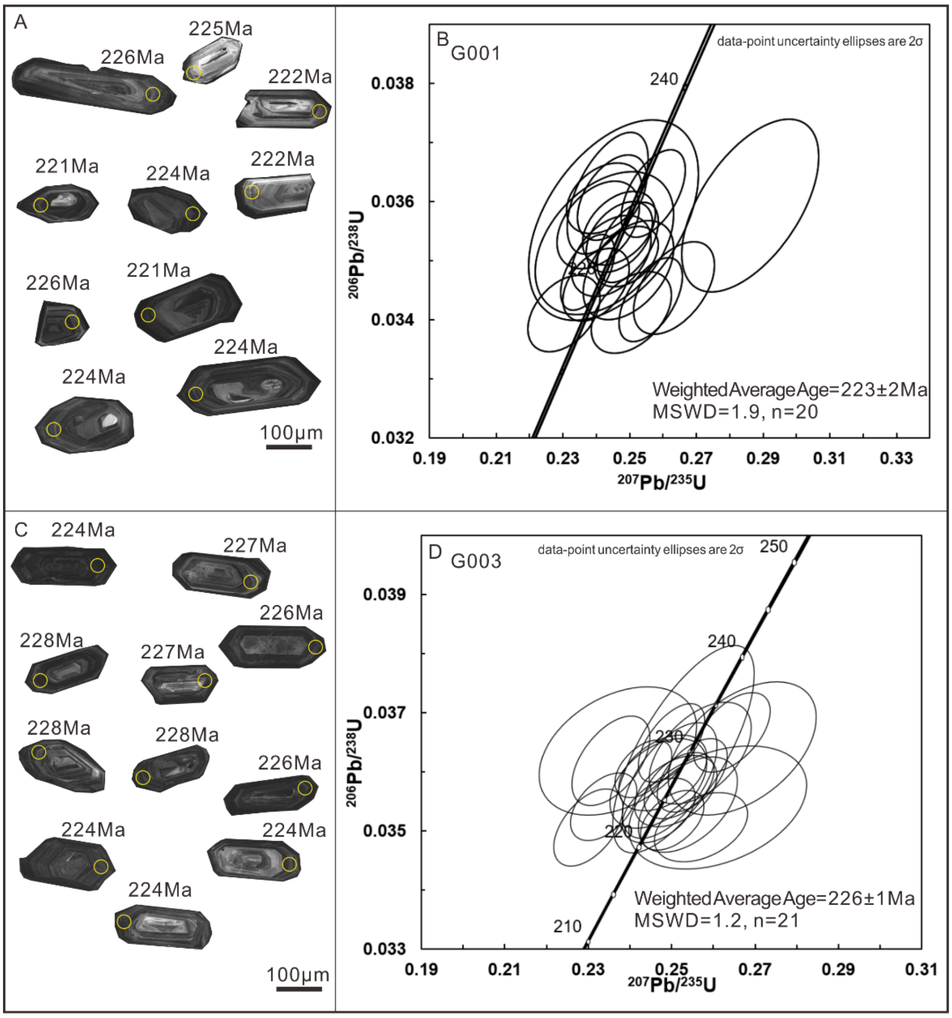

Figure 5. Typical CL images (**A**,**C**) and LA-ICP-MS zircon U-Pb concordant curves (**B**,**D**) of zircon of Baishi granite. The yellow, solid-line circles represent the locations of zircon U-Pb.

Twenty spot analyses on sample G001 yielded a weighted mean $^{206}U/^{238}Pb$ age of 223 ± 2 Ma (MSWD = 1.9) (Figure 5B). Twenty-one spot analyses on sample G003 yielded a weighted mean $^{206}U/^{238}Pb$ age of 226 ± 1 Ma (MSWD = 1.2) (Figure 5D). These ages were interpreted as the crystallization ages.

6.3. LA-ICP-MS Monazite U-Pb Dating and Rare Earth Elements Analysis

The LA-ICP-MS analyses using monazite U-Pb isotopes were conducted on two granite samples. The results are summarized in Table 2.

Table 1. LA-ICP-MS zircon U-Pb dating data of Baishi granite.

Analysis Spot	Th	U	Th/U	Isotope Ratios						Isotope Ages (Ma)					
	(ppm)	(ppm)		$^{207}Pb/^{206}Pb$	1σ	$^{207}Pb/^{235}U$	1σ	$^{206}Pb/^{238}U$	1σ	$^{207}Pb/^{206}Pb$	2σ	$^{207}Pb/^{235}U$	2σ	$^{206}Pb/^{238}U$	2σ
G001-ZR1-01	99	593	0.17	0.0527	0.0015	0.2505	0.0079	0.0341	0.0005	322	120	227	12	216	6
G001-ZR1-02	208	395	0.53	0.0579	0.0027	0.2862	0.0136	0.0359	0.0010	528	208	256	22	228	12
G001-ZR1-03	129	151	0.86	0.0501	0.0034	0.2452	0.0168	0.0357	0.0011	211	314	223	28	226	14
G001-ZR1-04	287	395	0.73	0.0507	0.0017	0.2468	0.0072	0.0355	0.0004	228	156	224	12	225	6
G001-ZR1-05	120	380	0.32	0.0486	0.0015	0.2424	0.0074	0.0361	0.0004	128	144	220	12	228	4
G001-ZR1-06	186	647	0.29	0.0505	0.0016	0.2445	0.0079	0.0351	0.0005	217	148	222	12	222	6
G001-ZR1-07	197	606	0.33	0.0502	0.0014	0.2399	0.0066	0.0346	0.0004	206	194	218	10	219	6
G001-ZR1-08	258	769	0.34	0.0494	0.0012	0.2374	0.0054	0.0348	0.0004	165	112	216	8	221	6
G001-ZR1-09	225	578	0.39	0.0490	0.0014	0.2303	0.0071	0.0341	0.0004	150	140	210	12	216	6
G001-ZR1-10	154	505	0.30	0.0536	0.0017	0.2633	0.0080	0.0345	0.0005	354	154	237	12	219	6
G001-ZR1-11	358	438	0.82	0.0501	0.0030	0.2424	0.0137	0.0353	0.0008	198	290	220	22	224	10
G001-ZR1-12	147	793	0.19	0.0510	0.0013	0.2491	0.0062	0.0351	0.0003	243	114	226	10	222	4
G001-ZR1-13	140	395	0.35	0.0488	0.0017	0.2406	0.0081	0.0356	0.0005	200	160	219	14	226	6
G001-ZR1-14	174	809	0.21	0.0488	0.0016	0.2434	0.0080	0.0361	0.0007	139	160	221	14	229	8
G001-ZR1-15	180	329	0.55	0.0525	0.0021	0.2497	0.0089	0.0348	0.0006	306	178	226	14	221	6
G001-ZR1-16	269	991	0.27	0.0510	0.0013	0.2494	0.0060	0.0353	0.0004	239	110	226	10	224	6
G001-ZR1-17	255	656	0.39	0.0517	0.0014	0.2571	0.0064	0.0361	0.0005	272	122	232	10	229	6
G001-ZR1-18	138	634	0.22	0.0504	0.0014	0.2468	0.0066	0.0354	0.0004	213	130	224	10	224	4
G001-ZR1-19	170	487	0.35	0.0540	0.0014	0.2563	0.0063	0.0343	0.0005	372	110	232	10	218	6
G001-ZR1-20	177	799	0.22	0.0489	0.0013	0.2447	0.0068	0.0361	0.0005	143	126	222	12	228	6
G003-ZR1-01	94	554	0.17	0.0529	0.0032	0.2608	0.0140	0.0354	0.0007	324	278	235	22	224	8
G003-ZR1-02	176	754	0.23	0.0524	0.0020	0.2667	0.0117	0.0364	0.0007	306	170	240	18	230	10
G003-ZR1-03	449	2238	0.20	0.0499	0.0014	0.2493	0.0075	0.0358	0.0006	191	134	226	12	227	8
G003-ZR1-04	108	1408	0.08	0.0501	0.0018	0.2525	0.0112	0.0364	0.0012	211	166	229	18	230	14
G003-ZR1-05	157	1035	0.15	0.0512	0.0012	0.2547	0.0055	0.0359	0.0004	250	112	230	8	228	6
G003-ZR1-06	193	1169	0.17	0.0469	0.0013	0.2353	0.0062	0.0362	0.0005	43	134	215	10	229	6

Table 1. *Cont.*

Analysis Spot	Th (ppm)	U (ppm)	Th/U	Isotope Ratios						Isotope Ages (Ma)					
				$^{207}Pb/^{206}Pb$	1σ	$^{207}Pb/^{235}U$	1σ	$^{206}Pb/^{238}U$	1σ	$^{207}Pb/^{206}Pb$	2σ	$^{207}Pb/^{235}U$	2σ	$^{206}Pb/^{238}U$	2σ
G003-ZR1-07	110	498	0.22	0.0498	0.0016	0.2465	0.0076	0.0358	0.0005	187	152	224	12	227	6
G003-ZR1-08	541	1389	0.39	0.0507	0.0012	0.2517	0.0055	0.0358	0.0004	233	108	228	8	226	4
G003-ZR1-09	281	670	0.42	0.0496	0.0014	0.2476	0.0070	0.0360	0.0004	176	130	225	12	228	6
G003-ZR1-10	150	2241	0.07	0.0485	0.0009	0.2430	0.0045	0.0360	0.0003	124	88	221	8	228	4
G003-ZR1-11	256	2353	0.11	0.0512	0.0011	0.2499	0.0050	0.0352	0.0003	256	96	227	8	223	4
G003-ZR1-12	180	925	0.19	0.0528	0.0015	0.2568	0.0073	0.0351	0.0004	320	134	232	12	222	4
G003-ZR1-13	227	937	0.24	0.0507	0.0013	0.2508	0.0065	0.0357	0.0004	233	118	227	10	226	6
G003-ZR1-14	154	921	0.17	0.0518	0.0016	0.2536	0.0078	0.0354	0.0005	276	136	230	12	224	6
G003-ZR1-15	114	1503	0.08	0.0503	0.0012	0.2467	0.0058	0.0353	0.0004	209	112	224	10	224	4
G003-ZR1-16	169	1928	0.09	0.0520	0.0012	0.2643	0.0060	0.0367	0.0004	283	112	238	10	232	6
G003-ZR1-17	675	1854	0.36	0.0492	0.0010	0.2497	0.0052	0.0365	0.0004	167	88	226	8	231	6
G003-ZR1-18	204	389	0.52	0.0469	0.0023	0.2368	0.0124	0.0364	0.0007	56	222	216	20	230	8
G003-ZR1-19	169	601	0.28	0.0478	0.0014	0.2298	0.0055	0.0350	0.0004	100	146	210	10	222	6
G003-ZR1-20	805	1595	0.50	0.0475	0.0010	0.2335	0.0052	0.0354	0.0004	72	104	213	8	224	4
G003-ZR1-21	152	797	0.19	0.0510	0.0017	0.2566	0.0080	0.0363	0.0006	243	152	232	12	230	8

Table 2. LA-ICP-MS monazite U-Pb dating data of Baishi granite.

Analysis Spot	Th	U	Th/U	Isotope Ratios						Isotope Ages (Ma)					
	(ppm)	(ppm)		$^{207}Pb/^{206}Pb$	1σ	$^{207}Pb/^{235}U$	1σ	$^{206}Pb/^{238}U$	1σ	$^{207}Pb/^{206}Pb$	2σ	$^{207}Pb/^{235}U$	2σ	$^{206}Pb/^{238}U$	2σ
G001-TW1-01	58,252	699	83.4	0.0566	0.0037	0.2818	0.0164	0.0370	0.0006	476	288	252	26	234	8
G001-TW1-02	57,159	788	72.5	0.0524	0.0030	0.2518	0.0150	0.0352	0.0005	302	262	228	24	223	6
G001-TW1-03	59,488	782	76.0	0.0502	0.0032	0.2400	0.0150	0.0352	0.0005	211	294	218	24	223	6
G001-TW1-04	58,987	695	84.9	0.0507	0.0032	0.2392	0.0146	0.0349	0.0005	233	290	218	24	221	6
G001-TW1-05	60,587	550	110.3	0.0527	0.0037	0.2570	0.0173	0.0360	0.0007	322	332	232	28	228	8
G001-TW1-06	64,042	2318	27.6	0.0492	0.0017	0.2456	0.0086	0.0363	0.0004	167	162	223	14	230	4
G001-TW1-07	56,577	658	85.9	0.0492	0.0035	0.2341	0.0154	0.0356	0.0006	167	300	214	26	226	8
G001-TW1-08	65,142	1556	41.9	0.0474	0.0020	0.2298	0.0098	0.0353	0.0004	78	182	210	16	224	4
G001-TW1-09	53,620	445	120.6	0.0559	0.0043	0.2763	0.0202	0.0368	0.0011	450	280	248	32	233	14
G001-TW1-10	55,868	476	117.4	0.0565	0.0048	0.2774	0.0219	0.0366	0.0007	472	316	249	34	232	8
G001-TW1-11	74,521	6945	10.7	0.0509	0.0012	0.2454	0.0058	0.0350	0.0003	235	112	223	10	222	4
G001-TW1-12	66,464	766	86.8	0.0528	0.0028	0.2703	0.0144	0.0374	0.0005	320	244	243	24	237	6
G001-TW1-13	58,121	532	109.2	0.0580	0.0038	0.2842	0.0166	0.0363	0.0007	532	344	254	26	230	8
G001-TW1-14	66,003	1567	42.1	0.0546	0.0022	0.2622	0.0104	0.0350	0.0004	394	178	236	16	222	4
G001-TW1-15	66,785	849	78.7	0.0568	0.0030	0.2753	0.0138	0.0355	0.0005	483	234	247	22	225	6
G001-TW1-16	65,960	1276	51.7	0.0511	0.0033	0.2416	0.0153	0.0346	0.0005	243	284	220	26	219	6
G001-TW1-17	60,359	736	82.0	0.0567	0.0040	0.2643	0.0169	0.0347	0.0005	480	310	238	28	220	6
G001-TW1-18	69,072	4283	16.1	0.0527	0.0015	0.2506	0.0072	0.0345	0.0003	317	138	227	12	219	4
G001-TW1-19	59,066	728	81.1	0.0560	0.0034	0.2712	0.0163	0.0351	0.0005	454	262	244	26	223	6
G001-TW1-20	60,604	815	74.3	0.0541	0.0034	0.2571	0.0150	0.0349	0.0005	376	278	232	24	221	6
G001-TW1-21	68,974	1569	44.0	0.0542	0.0022	0.2682	0.0115	0.0359	0.0004	376	194	241	18	227	6
G001-TW1-22	66,618	1351	49.3	0.0516	0.0028	0.2489	0.0124	0.0355	0.0005	333	248	226	20	225	6
G001-TW1-23	65,277	1414	46.2	0.0519	0.0023	0.2502	0.0110	0.0352	0.0004	283	212	227	18	223	4
G001-TW1-24	61,789	1362	45.4	0.0504	0.0024	0.2543	0.0114	0.0371	0.0007	217	218	230	18	235	8
G001-TW1-25	74,816	7363	10.2	0.0507	0.0011	0.2497	0.0055	0.0358	0.0003	228	104	226	8	227	4

Table 2. *Cont.*

Analysis Spot	Th (ppm)	U (ppm)	Th/U	Isotope Ratios						Isotope Ages (Ma)					
				$^{207}Pb/^{206}Pb$	1σ	$^{207}Pb/^{235}U$	1σ	$^{206}Pb/^{238}U$	1σ	$^{207}Pb/^{206}Pb$	2σ	$^{207}Pb/^{235}U$	2σ	$^{206}Pb/^{238}U$	2σ
G003-TW1-01	58,890	1259	46.8	0.0498	0.0027	0.2423	0.0125	0.0358	0.0005	183	260	220	20	227	6
G003-TW1-02	62,629	1348	46.5	0.0549	0.0026	0.2740	0.0120	0.0366	0.0005	409	220	246	20	232	6
G003-TW1-03	52,470	1075	48.8	0.0513	0.0038	0.2470	0.0167	0.0357	0.0008	254	340	224	28	226	10
G003-TW1-04	53,820	1142	47.1	0.0564	0.0027	0.2772	0.0132	0.0361	0.0005	478	206	248	20	229	6
G003-TW1-05	60,059	1832	32.8	0.0507	0.0022	0.2430	0.0105	0.0348	0.0004	228	200	221	18	221	6
G003-TW1-06	66,584	3382	19.7	0.0507	0.0017	0.2488	0.0078	0.0357	0.0003	233	152	226	12	226	4
G003-TW1-07	57,282	1082	52.9	0.0538	0.0029	0.2596	0.0139	0.0353	0.0005	361	248	234	22	223	6
G003-TW1-08	60,678	1987	30.5	0.0539	0.0022	0.2573	0.0104	0.0348	0.0004	369	186	232	16	220	6
G003-TW1-09	61,815	1642	37.6	0.0498	0.0024	0.2372	0.0113	0.0347	0.0004	187	216	216	18	220	6
G003-TW1-10	72,610	2898	25.1	0.0486	0.0019	0.2354	0.0093	0.0350	0.0003	128	182	215	16	222	4
G003-TW1-11	61,572	1915	32.2	0.0550	0.0028	0.2592	0.0128	0.0344	0.0004	413	230	234	20	218	6
G003-TW1-12	65,090	2345	27.8	0.0535	0.0021	0.2588	0.0094	0.0353	0.0004	350	174	234	16	223	4
G003-TW1-13	55,483	1165	47.6	0.0545	0.0028	0.2669	0.0130	0.0360	0.0005	391	168	240	20	228	6
G003-TW1-14	59,880	2052	29.2	0.0544	0.0027	0.2798	0.0136	0.0376	0.0006	387	218	250	22	238	6
G003-TW1-15	56,294	1358	41.5	0.0520	0.0027	0.2547	0.0131	0.0357	0.0005	287	306	230	22	226	6
G003-TW1-16	58,402	1683	34.7	0.0508	0.0025	0.2417	0.0112	0.0350	0.0004	228	230	220	18	222	4
G003-TW1-17	62,968	1505	41.8	0.0512	0.0030	0.2513	0.0144	0.0355	0.0005	250	280	228	24	225	6
G003-TW1-18	51,037	1148	44.4	0.0514	0.0027	0.2441	0.0125	0.0347	0.0005	261	176	222	20	220	6
G003-TW1-19	60,907	1636	37.2	0.0502	0.0024	0.2420	0.0112	0.0350	0.0003	206	222	220	18	222	4
G003-TW1-20	53,503	922	58.0	0.0552	0.0030	0.2653	0.0145	0.0350	0.0005	420	244	239	24	222	6
G003-TW1-21	58,839	1440	40.9	0.0585	0.0029	0.2745	0.0128	0.0345	0.0004	546	218	246	20	219	4
G003-TW1-22	63,637	1557	40.9	0.0583	0.0030	0.2808	0.0143	0.0349	0.0004	543	216	251	22	221	6
G003-TW1-23	54,987	1085	50.7	0.0770	0.0035	0.3850	0.0171	0.0366	0.0005	1122	180	331	26	232	6

BSE images of the representative monazite grains with $^{206}Pb/^{238}U$ ages are shown in Figure 6. The monazites were generally euhedral–subhedral, short-to-long prismatic, colorless, and transparent. The crystal length ranged from 100 to 500 μm, with length-to-width ratios of 1:1 to 3:1. The structure of most monazites was uniform without zonation, and the edge of the monazite grain was round (Figure 6A,C). The monazites showed variable U (445–7363 ppm) and Th (51,037–74,816 ppm) concentrations, with Th/U ratios ranging from 10.2 to 120.6 (Table 2).

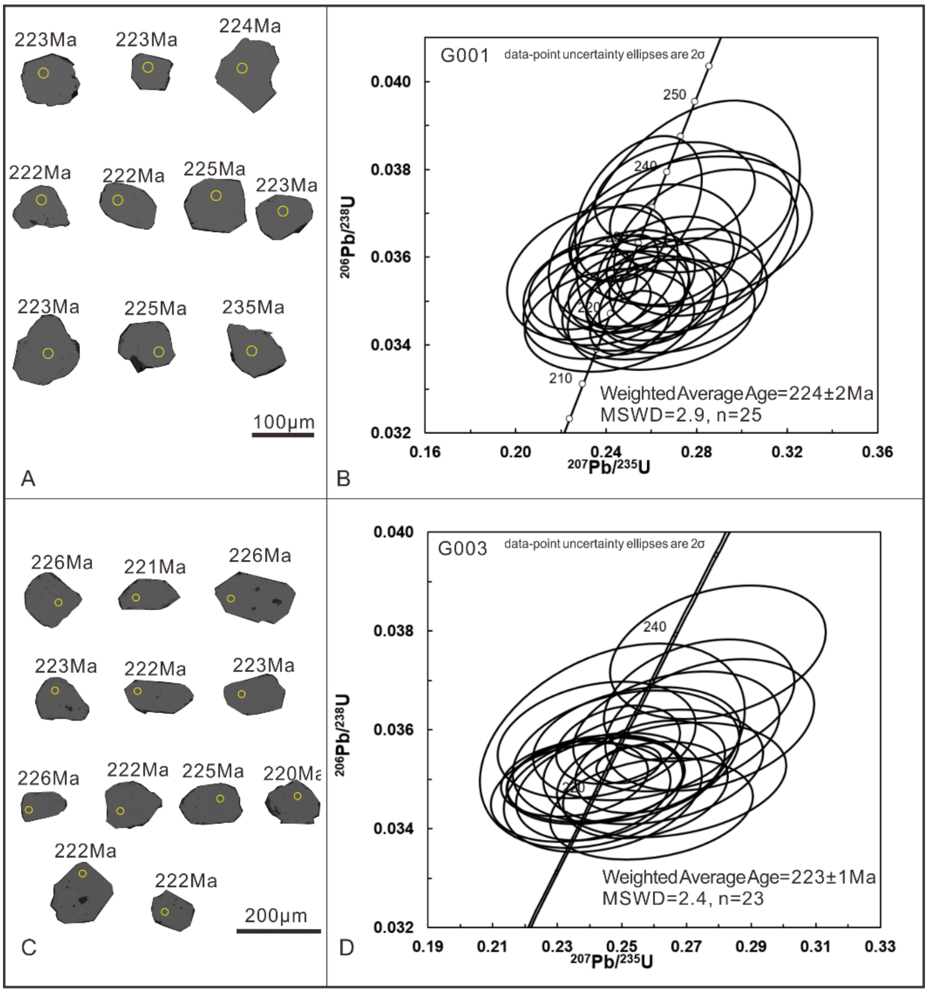

Figure 6. Typical BSE images (**A**,**C**) and LA-ICP-MS monazite U-Pb concordant curves (**B**,**D**) of monazite of Baishi granite. The yellow, solid-line circle represents the locations for monazite U-Pb.

Twenty-five spot analyses of sample G001 yielded a weighted mean $^{206}U/^{238}Pb$ age of 224 ± 2 Ma (MSWD = 2.9) (Figure 6B). Twenty-three spot analyses of sample G003 yielded a weighted mean $^{206}U/^{238}Pb$ age of 223 ± 1 Ma (MSWD = 5.2) (Figure 6D). The ages were interpreted as the crystallization ages.

In addition, the analysis of rare earth elements was conducted simultaneously, and the results are shown in Table 3. The samples display negative Eu anomalies (Figure 7).

Table 3. LA-ICP-MS monazite rare earth elements data of Baishi granite ($\times 10^{-6}$).

Analysis Spot	La	Ce	Pr	Nd	Sm	Eu	Gd	Tb	Dy	Ho	Er	Tm	Yb	Lu
G001-TW1-01	148,861	244,562	24,175	83,666	9499	164	4643	437	1590	211	344	27.7	96.4	9.28
G001-TW1-02	146,503	243,989	24,675	84,137	9975	180	5073	475	1764	235	392	31.7	113	11.0
G001-TW1-03	144,860	245,418	24,793	86,510	10,237	171	5209	498	1878	243	407	33.0	126	11.0
G001-TW1-04	139,383	243,502	24,807	89,315	11,067	196	5882	566	2126	293	480	36.8	144	12.3
G001-TW1-05	149,388	243,374	24,350	85,088	9655	198	4904	449	1692	224	366	27.9	104	10.1
G001-TW1-06	128,564	232,039	24,874	91,004	13,144	240	7703	840	3506	488	848	71.6	281	24.2
G001-TW1-07	143,731	245,909	24,644	86,332	9917	191	4968	458	1690	225	369	27.7	103	8.75
G001-TW1-08	133,537	238,185	25,213	91,756	12,095	244	6633	657	2601	355	603	49.6	179	17.0
G001-TW1-09	153,041	248,233	24,406	82,784	9034	176	4304	373	1386	180	293	22.7	87.4	7.95
G001-TW1-10	155,670	249,763	24,112	81,663	8558	152	4107	362	1336	173	281	22.3	82.4	7.76
G001-TW1-11	107,969	215,827	24,476	94,575	16,552	219	10,351	1195	4858	648	1127	95.6	396	33.3
G001-TW1-12	151,851	243,415	23,966	82,292	8827	165	4358	401	1513	207	336	26.5	111	9.45
G001-TW1-13	155,636	246,922	23,851	81,300	8580	157	4059	352	1303	168	279	21.7	83.6	6.77
G001-TW1-14	128,634	235,847	25,168	90,910	12,824	171	7030	703	2667	358	590	47.1	178	15.9
G001-TW1-15	137,995	239,094	24,733	88,746	11,501	234	5873	546	1879	229	343	24.5	89.6	7.24
G001-TW1-16	130,740	238,049	25,306	90,713	12,366	159	6777	686	2701	375	618	49.3	188	15.0
G001-TW1-17	142,305	242,842	24,338	85,159	9994	155	5034	484	1820	241	394	30.5	114	9.86
G001-TW1-18	120,567	225,264	24,429	91,030	14,690	198	8819	1015	4022	548	924	79.5	310	30.4
G001-TW1-19	142,168	245,853	25,127	89,914	10,894	208	5524	522	1894	252	419	32.4	121	11.7
G001-TW1-20	138,813	237,522	24,555	90,384	11,204	237	6198	607	2323	315	520	41.6	155	14.3
G001-TW1-21	131,306	237,582	24,525	88,910	11,878	144	6435	653	2596	355	597	48.9	189	16.6
G001-TW1-22	136,087	240,449	24,628	89,301	11,473	153	6124	615	2352	315	536	43.7	171	15.6
G001-TW1-23	131,769	235,418	24,596	89,538	11,967	189	6372	650	2570	350	595	48.4	179	16.6
G001-TW1-24	134,133	235,540	23,827	87,171	10,937	192	5976	595	2313	316	533	44.4	171	15.4
G001-TW1-25	105,849	210,068	23,782	90,394	16,345	197	10,643	1344	5755	810	1477	133	567	51.7
G003-TW1-01	136,336	239,779	25,106	90,193	11,710	169	6048	600	2318	316	525	41.2	154	13.9
G003-TW1-02	135,854	241,237	25,085	90,586	11,978	163	6127	595	2231	301	494	40.3	151	12.8
G003-TW1-03	140,653	244,072	25,154	89,345	11,776	203	6125	602	2257	303	480	39.9	143	12.9
G003-TW1-04	143,307	244,390	25,062	89,222	11,394	191	5857	568	2175	283	467	37.0	142	12.4
G003-TW1-05	127,852	239,371	25,392	92,533	13,208	140	7192	750	2999	412	705	57.4	221	19.6
G003-TW1-06	111,582	224,165	25,758	98,883	16,249	269	9137	977	3969	543	927	76.7	291	26.4
G003-TW1-07	137,815	242,739	25,083	88,599	11,518	169	6044	582	2241	304	495	40.1	152	13.4
G003-TW1-08	126,539	230,630	25,078	92,444	13,680	250	7712	803	3176	435	724	57.7	230	19.6
G003-TW1-09	129,026	235,448	25,315	92,911	13,321	205	7413	750	2964	393	643	49.7	190	16.2
G003-TW1-10	115,329	228,963	25,474	94,126	15,182	193	8529	907	3634	502	858	71.0	282	23.9
G003-TW1-11	136,153	239,310	24,755	84,793	11,493	179	5864	535	1820	197	232	14.5	42.1	3.16
G003-TW1-12	125,219	233,759	24,908	90,142	13,357	178	7460	791	3203	444	754	62.9	253	22.3
G003-TW1-13	138,522	241,732	24,998	90,846	11,815	186	6314	611	2338	302	495	37.6	144	12.5
G003-TW1-14	127,032	232,872	25,094	92,678	13,303	173	7244	755	2972	410	706	58.2	223	20.3
G003-TW1-15	133,141	238,994	25,187	92,334	12,433	210	6705	665	2554	344	566	44.5	173	14.2
G003-TW1-16	133,987	241,309	25,256	90,335	12,744	153	6921	713	2798	382	646	51.9	207	16.7
G003-TW1-17	131,910	240,218	25,483	92,353	12,606	178	6513	627	2441	328	551	43.3	165	15.3
G003-TW1-18	140,758	244,113	25,363	92,040	11,896	193	6230	603	2313	304	507	39.1	146	13.1
G003-TW1-19	131,353	236,412	25,126	92,754	12,844	186	7073	719	2864	392	663	53.9	198	18.9
G003-TW1-20	146,753	248,219	24,922	86,450	10,543	198	5358	500	1897	249	401	31.6	119	10.0
G003-TW1-21	136,580	243,321	25,215	88,712	12,236	200	6586	625	2192	267	396	28.5	103	8.66
G003-TW1-22	130,692	237,202	24,830	89,340	12,449	152	6735	668	2680	353	608	48.1	172	16.3
G003-TW1-23	140,700	244,169	24,776	88,517	11,216	174	5790	556	2125	285	468	37.4	137	13.3

7. Discussion

7.1. Origin of Monazite

In terms of genetic mineralogy, monazites can be divided into magmatic monazite, metamorphic monazite, and hydrothermal monazite. It is very important to identify the monazite genetic types for the reasonable explanation of U-Pb ages. The types of monazites can be distinguished according to paragenetic minerals, BSE characteristics, and rare earth element characteristics [38].

Magmatic monazite often exhibits oscillating bands [39], fan-shaped zones [40], and homogeneous internal structures [41] in BSE images, with few inclusions. The common internal structures of hydrothermal monazite in BSE images are concentric oscillating bands and fan-shaped zonings, and a large number of fluid inclusions are developed inside [42]. In this study, a single monazite particle selected from Baishi pluton showed a homogeneous structure in the BSE image (Figure 5A,C), with very few internal inclusions, so it was presumed to be magmatic monazite.

From the perspective of the rare earth element characteristics of monazite, magmatic monazite usually has obvious negative Eu anomalies, while hydrothermal monazite has no Eu anomalies or no obvious negative Eu anomalies [38]. The chondrite-normalized rare earth elements of monazite in this study were compared with data of typical magmatic monazite and hydrothermal monazite (Table 3, Figure 7), further confirming that the monazite in this study was of the magmatic type because of the similar patterns between the monazite in this study and magmatic monazite. Therefore, the age of monazite obtained in this paper could represent the age of formation of Baishi granite, which intruded in the late Triassic.

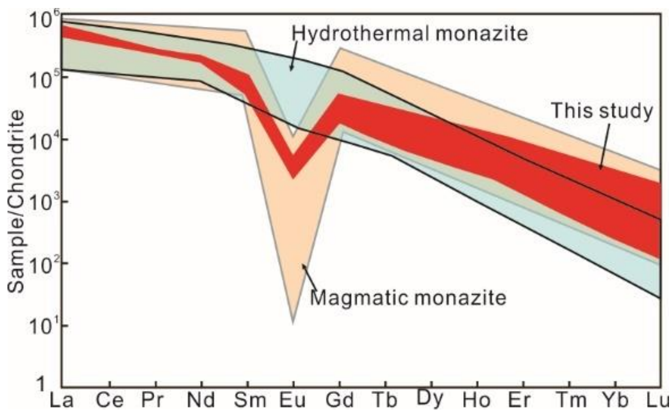

Figure 7. Normalized REE pattern of Baishi granite monazite. Chondrite data are from [43]. The red filled area represents the data of this study. The blue transparent area represents hydrothermal monazite (data from [44]). The orange transparent area represents hydrothermal monazite (data from [41]).

7.2. Age of the Baishi W-Cu Deposit and Geodynamic Setting

There is much debate about the geodynamic setting of magmatism and mineralization during the Indosinian in South China. Compared with previous models of continental collision involving the westward subduction of the Pacific Plate [45–47] and the flat-slab subduction of the Paleo-Pacific plate [48], recently, researchers have tended toward the perspective of intracontinental orogeny [17,49,50]. Unfortunately, the absence of island arc granites [49,51] suggests that the early Mesozoic magmatic event is not directly related to plate subduction. However, there is much evidence to support the occurrence of an intracontinental tectonic event: (1) the large area distribution of bimodal vocanics generated in the setting of lithosphere extension and thinning [52], such as gabbro dating to 225 Ma in Daoxian in Hunan province and plagioclase amphibolite dating to 252 Ma in Jingning in Zhejiang province [53]; (2) the absence of early Mesozoic ophiolite, a subduction complex, related volcanic rocks, arc magmatism, and high-pressure metamorphism in South

China [49,51,54–56]; (3) the existence of quite a few mylonitized granites that formed later than the regional deformation action, suggesting that there was a process of extrusion and extension in the Triassic [57,58].

During the Indosinian, the South China plate was located between the North China plate and the Indo-China peninsula, and the Indosinian movement probably began in the middle Permian (267~262 Ma) [59]. The collision peak between the Indo-China peninsula and the South China block generated the Song Ma suture zone dated at 258~243 Ma [60]. Moreover, the metamorphic peak age of the Qinling–Dabie suture is 230~226 Ma, which represents the collision between the South China block and the North China block [61]. The collision force was transmitted from south to north, which may have been related to the sequential collision of the Indo-China peninsula, the South China block, and the North China block [60–62]. Indosinian orogeny completed the integration of the South China and North China blocks and formed a unified Chinese mainland. A series of collisions resulted in intense magmatism and mineralization in the domain. Although the Nanling region is located in the hinterland of South China, it is still affected by the remote effect of multiple block collisions [20].

Furthermore, research shows that the intense extension and deformation led to the crust thickness being increased by 50 km [60]. Additionally, the crust thickening caused crust extension and decompression melting, forming granite magma [63,64]. Many early–middle-Triassic syncollisional granites and late-Triassic post-collisional granites were generated in this area [65]. Against the extensional tectonic background, a series of tungsten–polymetallic mineralizations related to granites occurred [19,21,22].

The LA-ICP-MS zircon U-Pb ages of the ore-related Baishi granite of the Baishi W-Cu deposit were determined to be 223 ± 2 Ma and 226 ± 1 Ma, and the LA-ICP-MS U-Pb ages of the magmatic monazite were determined to be 224.6 ± 2.0 Ma and 223.7 ± 1.6 Ma. In consideration of the reliability of the dating methods and Baishi granite's tendency toward mineralization, it could be inferred that the Baishi W-Cu deposit was formed in the Triassic. On account of the age of formation of the rock, which is 226~223 Ma, it was inferred that the Baishi W-Cu deposit was formed in the extensional stage after intracontinental orogeny (Figure 8).

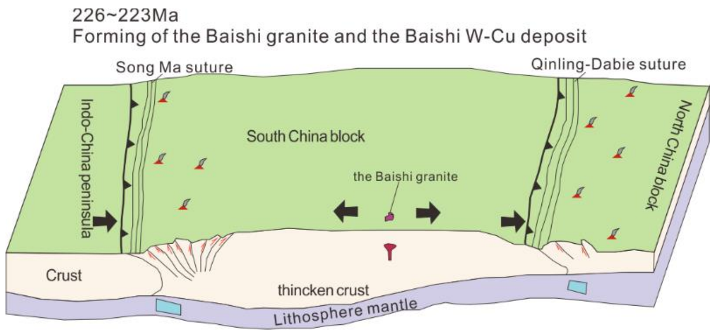

Figure 8. Geodynamic model for the forming of Baishi granite and the Baishi W-Cu deposit.

7.3. Indosinian Tungsten Mineralization in the Nanling Region

For a long time, the chronology of granites and related tungsten mineralization in the Nanling region has widely drawn the attention of geologists [9–11,17,65–70]. According to our statistics, more than 50 tungsten-related deposits in the Nanling metallogenic belt have been studied in detail, and many papers have been published [13,15,16,68,71,72] (Table 4, Figure 9). Most studies show that the majority of tungsten deposits in the Nanling region are related to granite intrusions in the Yanshanian [5–11]. However, Huang and Chen [73] put forward that although tungsten deposits in the Nanling region were mainly formed in the Yanshanian, they may have experienced multi-stage mineralization, especially during the Indosinian.

Table 4. Summary of chronological data on the major typical W polymetallic deposits in the Nanling region.

No.	Deposit	Mineralization	Age/Ma	Method of Dating	Reference
1	Dajishan, Southern Jiangxi	W-Nb-Ta	144	Mica Ar-Ar	[74]
2	Dajishan, Southern Jiangxi	W-Nb-Ta	147	Mica Ar-Ar	[75]
3	Yaoling, Northern Guangdong	W	149	Mica Ar-Ar	[75]
4	Niutangjie, Northern Guangxi	W	418	Apatite U-Pb	[76]
5	Hongshuizhai, Jiulongnao orefield, Southern Jiangxi	W	156	Molybdenite Re-Os	[77]
6	Jiulongnao, Jiulongnao orefield, Southern Jiangxi	W	151	Molybdenite Re-Os	[77]
7	Zhangdongkeng, Jiulongnao orefield, Southern Jiangxi	W	151	Molybdenite Re-Os	[77]
8	Taoxikeng, Southern Jiangxi	W	152	Muscovite Ar-Ar	[78]
9	Taoxikeng, Southern Jiangxi	W	155	Muscovite Ar-Ar	[78]
10	Meiziwo, Northern Guangdong	W	156	Muscovite Ar-Ar	[79]
11	Zhangdongkeng, Southern Jiangxi	W	154	Molybdenite Re-Os	[80]
12	Jiaoli, Southern Jiangxi	W polymetallic	170	Molybdenite Re-Os	[81]
13	Baoshan, Southern Jiangxi	W	161	Molybdenite Re-Os	[81]
14	Dengfuxian, Hunan	W	152	Molybdenite Re-Os	[82]
15	Qingshiling, Southern Hunan	W-Mo	157	Quartz Rb-Sr	[83]
16	Dalingbei, Southern Hunan	W	150	Zinnwaldite Ar-Ar	[83]
17	Xihuashan, Southern Jiangxi	W	139	Quartz Rb-Sr	[84]
				Wolframite Sm-Nd	[84]
18	Xihuashan, Southern Jiangxi	W	137	Fluorite Sm-Nd	[84]
19	Niuling, Southern Jiangxi	W-Sn	154	Molybdenite Re-Os	[85]
20	Yaolanzhai, Southern Jiangxi	W	155	Molybdenite Re-Os	[8]
21	Jiangjunzhai, Southeast Hunan	W	169	Molybdenite Re-Os	[86]
22	Miao'ershan, Northern Guangxi	W	212	Scheelite Sm-Nd	[14]
23	Helong, Southern Jiangxi	W	157	Molybdenite Re-Os	[87]
24	Helong, Southern Jiangxi	W	159	Molybdenite Re-Os	[87]
25	Yanqian, Southern Jiangxi	W	159	Molybdenite Re-Os	[88]
26	Hongling, Guangdong	W	159	Molybdenite Re-Os	[89]
27	Yaogangxian, Hunan	W-Mo	156	Quartz Rb-Sr	[90]
28	Yaogangxian, Hunan	W-Mo	175	Quartz Rb-Sr	[90]
29	Yaogangxian, Hunan	W-Mo	170	Molybdenite Re-Os	[90]
30	Gao'aobei, Hunan	W	157	Molybdenite Re-Os	[90]
31	Yaogangxian, Hunan	W-Mo	158	Cassiterite U-Pb	[91]
32	Jianlong, Southern Jiangxi	Cu-W	155	Molybdenite Re-Os	[92]
33	Chuankou	W	212	Molybdenite Re-Os	[17]
				Wolframite U-Pb	[17]
34	Zhangjiadi, Southern Jiangxi	W	158	Molybdenite Re-Os	[18]
35	Zhangjiadi, Southern Jiangxi	W	161	Molybdenite Re-Os	[18]
36	Shizhuyuan, Hunan	W-Mo-Bi	153	Muscovite Ar-Ar	[93]
37	Shizhuyuan, Hunan	W-Mo-Bi	152	Quartz Ar-Ar	[93]
38	Da'ao, Southern Hunan	W-Sn	151	Molybdenite Re-Os	[94]
39	Xintianling, Southern Hunan	W-Mo	161	Molybdenite Re-Os	[95]

Table 4. *Cont.*

No.	Deposit	Mineralization	Age/Ma	Method of Dating	Reference
40	Zhazixi, Hunan	W-Sb	227	Scheelite Sm-Nd	[96]
41	Anjiatan, Southern Jiangxi	W-Bi-Mo	156	Molybdenite Re-Os	[97]
42	Yuanlingzhai, Southern Jiangxi	W-Bi-Mo	160	Molybdenite Re-Os	[97]
43	Zhangdou, Southern Jiangxi	W-Sn	149	Molybdenite Re-Os	[95]
44	Huangsha, Southern Jiangxi	W	153	Molybdenite Re-Os	[98]
45	Piaotang, Gannan	W-Sn	158	Muscovite Ar-Ar	[12]
46	Keshuling, Gannan	W-Sn	158	Muscovite Ar-Ar	[12]
47	Xian'etang, Gannan	Sn-W	231	Muscovite Ar-Ar	[12]
48	Qingshan, Jiangxi	W	228	Muscovite Ar-Ar	[16]
49	Qingshan, Jiangxi	W	229	Muscovite Ar-Ar	[16]
50	Baxiannao, Southern Jiangxi	W-Sn-Mo-Bi	158	Cassiterite U-Pb	[99]
51	Bikeng, Southern Jiangxi	W-Sn-Mo-Bi	159	Cassiterite U-Pb	[99]
52	Jinzhuping, Southern Jiangxi	W-Sn-Mo-Bi	156	Cassiterite U-Pb	[99]
53	Jinzhuping, Southern Jiangxi	W-Sn-Mo-Bi	157	Molybdenite Re-Os	[99]
54	Changkeng, Southern Jiangxi	W-Sn	156	Cassiterite U-Pb	[55]
55	Maoping, Southern Jiangxi	W-Sn	156	Cassiterite U-Pb	[11]
56	Xiangdong, Hunan	W-Sn	151	Cassiterite U-Pb	[71]
57	Xiangdong, Hunan	W-Sn	141	Cassiterite U-Pb	[71]
58	Xiangdong, Hunan	W-Sn	136	Cassiterite U-Pb	[71]
59	Sanjiaotan, Hunan	W	225	Molybdenite Re-Os	[15]
60	Baishi, Jiangxi	W-Cu	223	Zircon U-Pb Monazite U-Pb	This study
			224	Monazite U-Pb	
			226	Zircon U-Pb	

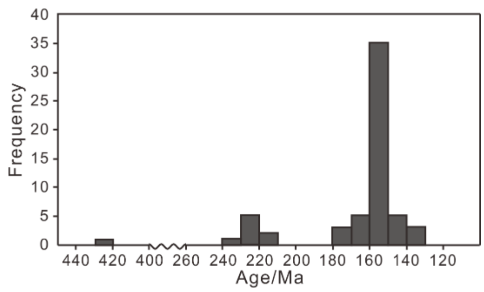

Figure 9. The metallogenic age of the tungsten polymetallic deposits in the Nanling region (detailed reference in Table 4).

In recent years, increasing numbers of researchers have discovered Indosinian tungsten deposits in the Nanling region based on the quick development of dating technology ([12–17], this study). In addition, more scholars have realized that the tungsten mineralization in the Nanling region is characterized by multiple stages [4,18]. Mao et al. [4] systematically summarize the high-precision isotopic chronology data published in recent years and divide the Mesozoic tungsten polymetallic mineralization in the Nanling region into three stages, finding the Yanshanian to be the peak stage of mineralization. Meanwhile, the Indosinian has become increasingly important when discussing tungsten mineralization in the Nanling metallogenic belt. However, insufficient attention has been paid to the exploration of tungsten mineralization in the Indosinian.

This study provides new data relating to Indosinian mineralization in the Nanling metallogenic belt, further proving that the Indosinian has prospecting potential. Geologists should pay more attention to strengthening Indosinian tungsten prospecting in the Nanling region.

8. Conclusions

1. The zircon and monazite LA-ICP-MS U-Pb dating results can confirm the chronology of the ore-related Baishi granite, which formed in late Triassic, ranging from 226 to 223 Ma;
2. The Baishi W-Cu deposit was formed in an extensional environment after intracontinental orogeny;
3. Indosinian tungsten mineralization in the Nanling region has great exploration potential.

Author Contributions: Conceptualization, L.L. and H.-L.L.; methodology, L.L. and H.-L.L.; formal analysis, H.-L.L.; investigation, H.-L.L. and J.-D.S.; writing—original draft, L.L. and H.-L.L.; writing—review and editing, L.L. and G.-G.W.; founding acquisition, L.L. and J.-D.S. All authors have read and agreed to the published version of the manuscript.

Funding: This work was financially supported by the open fund of State Key Laboratory for Mineral Deposits Research, Nanjing University (grant No. 2022-LAMD-K09); National Science Foundation of the Jiangsu Higher Education Institutions of China (grant No. 22KJD170001); China Geological Survey Program (grant No. DD20221688); Engineering Research Center Program of Development & Reform Commission of Jiangsu Province (grant No. [2021] 1368); and Nature Science Research Project of Jiangsu Urban and Rural Construction College (grant No. XJZK21013).

Data Availability Statement: Not Applicable.

Acknowledgments: We express our thanks to anonymous reviewers for their constructive comments, which significantly improved the manuscript. The authors thank X.H.L. and C.L.Z. from Nanjing Center, China Geological Survey, and C.B.F. and Z.X.W. from Gannan Geological Brigade for their help during fieldwork. The authors thank State Key Laboratory for Mineral Deposits Research, Nanjing University, Nanjing Hongchuang Geological Exploration Technology Service Co., Ltd., and Wuhan SampleSolution Analytical Technology Co., Ltd., for their assistance in the experiment.

Conflicts of Interest: The authors declare no conflict of interest.

References

1. Chen, Y.C.; Pei, R.F.; Zhang, H.L. *The Geology of Nonferrous and Rare Metal Deposits Related to Mesozoic Granitoids in the Nanling Region, China*; Geological Press: Beijing, China, 1989. (In Chinese)
2. Pei, R.F.; Wang, Y.L.; Li, L.; Wang, H.L. South China Great Granite Province and Its Metallogenic Series of Tungsten-Tin Poly-metallics. *China Tungsten Ind.* **2008**, *23*, 10–13, (In Chinese with English Abstract).
3. Hua, R.M.; Chen, P.R.; Zhang, W.L.; Lu, J.J. Three major metallogenic events in Mesozoic in South China. *Miner. Depos.* **2005**, *24*, 99–107, (In Chinese with English Abstract).
4. Mao, J.W.; Cheng, Y.B.; Chen, M.H.; Franco, P. Major types and time-space distribution of Mesozoic ore deposits in South China and their geodynamic settings. *Miner. Depos.* **2013**, *48*, 267–294.
5. Peng, J.T.; Zhou, M.F.; Hu, R.Z.; Shen, N.P.; Yuan, S.D.; Bi, X.W.; Du, A.D.; Qu, W.J. Precise molybdenite Re-Os and mica Ar-Ar dating of the Mesozoic Yaogangxian tungsten deposit, central Nanling district, South China. *Miner. Depos.* **2006**, *41*, 661–669. [CrossRef]
6. Feng, C.Y.; Feng, Y.D.; Xu, J.X.; Zeng, Z.L.; She, H.Q.; Zhang, D.Q.; Qu, W.J.; Du, A.D. Isotope chronological evidence for Upper Jurassic petrogenesis and mineralization of altered granite-type tungsten deposits in the Zhangtiantang area, southern Jiangxi. *Geol. China* **2007**, *34*, 642–650, (In Chinese with English Abstract).
7. Li, G.L.; Hua, R.M.; Wei, X.L.; Wang, X.D.; Huang, X.E. Rb-Sr Isochron Age of Single-grain Muscovite in the Xushan W-Cu Deposit Central Jiangxi, and Its Geological Significance. *Earth Sci.-J. China Univ. Geosci.* **2011**, *36*, 282–288, (In Chinese with English Abstract).
8. Feng, C.Y.; Zeng, Z.L.; Zhang, D.Q.; Qu, W.J.; Du, A.D.; Li, D.X.; She, H.Q. SHRIMP zircon U-Pb and molybdenite Re-Os isotopic dating of the tungsten deposits in the Tianmenshan-Hongtaoling W-Sn orefield, southern Jiangxi Province, China, and geological implications. *Ore Geol. Rev.* **2011**, *43*, 8–25. [CrossRef]
9. Hu, R.Z.; Wei, W.F.; Bi, X.W.; Peng, J.T.; Qi, Y.Q.; Wu, L.Y.; Chen, Y.W. Molybdenite Re-Os and muscovite $^{40}Ar/^{39}Ar$ dating of the Xihuashan tungsten deposit, central Nanling district, South China. *Lithos* **2012**, *150*, 111–118. [CrossRef]

10. Zhou, Y.; Liang, X.Q.; Wu, S.C.; Cai, Y.C.; Liang, X.R.; Shao, T.B.; Wang, C.; Fu, J.G.; Jiang, Y. Isotopic geochemistry, zircon U-Pb ages and Hf isotopes of A-type granites from the Xitian W-Sn deposit, SE China: Constraints on petrogenesis and tectonic significance. *J. Asian Earth Sci.* **2015**, *105*, 122–139. [CrossRef]
11. Chen, L.L.; Ni, P.; Dai, B.Z.; Li, W.S.; Chi, Z.; Pan, J.Y. The Genetic Association between Quartz Vein- and Greisen-Type Mineralization at the Maoping W-Sn Deposit, Southern Jiangxi, China: Insights from Zircon and Cassiterite U-Pb Ages and Cassiterite Trace Element Composition. *Minerals* **2019**, *9*, 411. [CrossRef]
12. Liu, S.B.; Wang, D.H.; Chen, Y.C.; Li, J.K.; Ying, L.J.; Xu, J.X.; Zeng, Z.L. $^{40}Ar/^{39}Ar$ Ages of Muscovite from Different Types Tungsten-Bearing Quartz Veins in the Chong-Yu-You Concentrated Mineral Area in Gannan Region and Its Geological Significance. *Acta Geol. Sin.* **2008**, *82*, 932–940, (In Chinese with English Abstract).
13. Zhang, D.; Zhang, W.L.; Wang, R.C.; Chu, Z.Y.; Gong, M.W.; Jiang, G.X. Quartz-vein Type Tungsten Mineralization Associated with the Indosinian (Triassic) Gaoling Granite, Miao'ershan Area, Northern Guangxi. *Geol. Rev.* **2015**, *61*, 817–834, (In Chinese with English Abstract).
14. Zhang, R.Q.; Lu, J.J.; Wang, R.C.; Yang, P.; Zhu, J.C.; Yao, Y.; Gao, J.F.; Li, C.; Lei, Z.H.; Zhang, W.L.; et al. Constraints of in situ zircon and cassiterite U-Pb, molybdenite Re-Os and muscovite ^{40}Ar-^{39}Ar ages on multiple generations of granitic magmatism and related W-Sn mineralization in the Wangxianling area, Nanling Range, South China. *Ore Geol. Rev.* **2015**, *65*, 1021–1042. [CrossRef]
15. Peng, N.L.; Wang, X.H.; Yang, J.; Chen, D.; Luo, L.; Luo, P.; Liu, T.Y. Re-Os dating of molybdenite from Sanjiaotan tungsten deposit in Chuankou area, Hunan Province, and its geological implications. *Miner. Depos.* (In Chinese with English Abstract). **2017**, *36*, 1402–1414.
16. Zhao, Z.; Zhao, W.W.; Lu, L.; Wang, H.Y. Constraints of multiple dating of the Qingshan tungsten deposit on the Triassic W(-Sn) mineralization in the Nanling region, South China. *Ore Geol. Rev.* **2018**, *94*, 46–57. [CrossRef]
17. Li, W.S.; Ni, P.; Pan, J.Y.; Fan, M.S.; Chen, L.L.; Zhang, D.; Wu, X.W.; Gao, Y. Constraints on the timing and genetic link of scheelite- and wolframite-bearing quartz veins in the Chuankou W ore field, South China. *Ore Geol. Rev.* **2021**, *133*, 104122. [CrossRef]
18. Feng, C.Y.; Zeng, Z.L.; Qu, W.J.; Liu, J.S.; Li, H.P. A geochronological study of granite and related mineralization of the Zhangjiadi molybdenite-tungsten deposit in Xingguo County, southern Jiangxi Province, China, and its geological significance. *Acta Petrol. Sin.* **2015**, *31*, 709–724, (In Chinese with English Abstract).
19. Xie, G.Q.; Mao, J.W.; Zhang, C.Q.; Li, W.; Song, S.W.; Zhang, R.Q. Triassic deposits in South China: Geological characteristics, ore forming mechanism and ore deposit model. *Earth Sci. Front.* **2021**, *28*, 252–270, (In Chinese with English Abstract).
20. Mao, J.W.; Zhou, Z.H.; Feng, C.Y.; Wang, Y.T. A preliminary study of the Triassic large-scale mineralization in China and its geodynamic setting. *Geol. China* **2012**, *39*, 1437–1471, (In Chinese with English Abstract).
21. Wang, D.H.; Chen, Y.C.; Jiang, B.; Huang, F.; Wang, Y.; Li, H.Q.; Hou, K.J. Preliminary study on the Triassic continental mineralization system in China. *Earth Sci. Front.* **2020**, *27*, 45–59, (In Chinese with English Abstract).
22. Liang, H.Y.; Wu, J.; Sun, W.D.; Mo, J.H.; Huang, W.T. Discussion on Indosinian mineralization in South China. *Acta Mineral. Sin.* **2011**, *31* (Supp. S1), 53–54. (In Chinese)
23. Wu, Y.B.; Zheng, Y.F. Study on zircon in mineralogy and constraints on the interpretation of U-Pb ages. *Chin. Sci. Bull.* **2004**, *49*, 1589–1604. (In Chinese) [CrossRef]
24. Schulz, B. Monazite Microstructures and Their Interpretation in Petrochronology. *Front. Earth Sci.* **2021**, *9*, 668566. [CrossRef]
25. Erokhin, Y.H.; Khiller, V.V.; Ivanov, K.S. Detrital Monazite from Upper Jurassic Sediments in the Central Part of the Frolov Megadepression, Western Siberia: Chemical Dating and Provenances. *Lithol. Miner. Resour.* **2019**, *54*, 262–271. [CrossRef]
26. Parrish, R.R. U-Pb dating of monazite and its application to geological problems. *Can. J. Earth Sci.* **1990**, *27*, 1431–1450. [CrossRef]
27. Zhou, X.W.; Zhao, G.C.; Wei, C.J.; Geng, Y.S. Metamorphic evolution and Th-U-Pb zircon and monazite geochronology of high-pressure pelitic granulites in the Jiaobei massif of the North China Craton. *Am. J. Sci.* **2008**, *308*, 328–350. [CrossRef]
28. Xiong, Z.W.; Xu, H.J.; Wang, P.; Zhang, J.F. Monazite recorded Paleoproterozoic granulite-facies metamorphism and Triassic fluid modification of the Weihai pelitic granulite, Sulu orogen. *Sci. China Earth Sci.* **2021**, *64*, 932–950. [CrossRef]
29. Fan, C.H.; Ni, P.; Wang, G.G.; Zhang, K.H.; Wang, G.L.; Li, W.S.; Cui, J.M.; He, J.F. Accessory minerals U-Pb geochronology of monzogranitic porphyry in Yangchuling porphyry W-Mo deposit in northern of Jiangxi Province, South China. *Miner. Depos.* **2022**, *41*, 35–52, (In Chinese with English Abstract).
30. Li, X.H.; Li, W.X.; Wang, X.C.; Li, Q.L.; Liu, Y.; Tang, G.Q. Role of mantle-derived magma in genesis of early Yanshanian granites in the Nanling Range, South China: In situ zircon Hf-O isotopic constraints. *Sci. China Ser. D Earth Sci.* **2009**, *52*, 1262–1278. [CrossRef]
31. Liu, H.; Zhao, X.L.; Jiang, J.; Zhang, J.G.; Liu, M.Z. The formation mechanism of the Xingguo vortex structure and its geological implication for the Mesozoic sinistral strike-slip in South China Block. *Chin. J. Geol.* **2021**, *56*, 808–828, (In Chinese with English Abstract).
32. Wedepohl, K.H. The composition of the continental crust. *Geochem. Cosmochim.* **1995**, *59*, 1217–1232. [CrossRef]
33. Jiangxi Bureau of Geology and Mineral Resources. *Geological Mineral Map (Qingxi Village, 1:50000)*; Jiangxi Bureau of Geology and Mineral Resources: Nanchang, China, 1991.
34. Hrstka, T.; Gottlieb, P.; Skála, R.; Breiter, K.; Motl, D. Automated mineralogy and petrology—Applications of TESCAN Integrated Mineral Analyzer (TIMA). *J. Geosci.* **2018**, *63*, 47–63. [CrossRef]
35. Andersen, T. Correction of common lead in U-Pb analyses that do not report ^{204}Pb. *Chem. Geol.* **2002**, *192*, 59–79. [CrossRef]

36. Ludwig, K.R. *User's Manual for Isoplot/Ex (Rev. 2.49): A Geochronological Toolkit for Microsoft Excel*; Berkeley Geochronology Center Special Publication: Berkeley, CA, USA, 2001.
37. Williams, I.S.; Buick, I.S.; Cartwright, I. An extended episode of early Mesoproterozoic metamorphic fluid flow in the Reynolds Range, central Australia*. *J. Metamorph. Geol.* **1996**, *14*, 29–47. [CrossRef]
38. Liang, X.; Xu, Y.J.; Zi, J.W.; Zhang, H.C.; Du, Y.S. Genetic mineralogy of monazite and constraints on the interpretation of U-Th-Pb ages. *Earth Sci.* **2021**, *47*, 1383–1398, (In Chinese with English Abstract).
39. Crowley, J.L.; Brown, R.L.; Gervais, F.; Gibson, H.D. Assessing Inheritance of Zircon and Monazite in Granitic Rocks from the Monashee Complex, Canadian Cordillera. *J. Petrol.* **2008**, *49*, 1915–1929. [CrossRef]
40. Williams, M.L.; Jercinovic, M.J.; Hetherington, C.J. Microprobe Monazite Geochronology: Understanding Geologic Processes by Integrating Composition and Chronology. *Annu. Rev. Earth Planet. Sci.* **2007**, *35*, 137–175. [CrossRef]
41. Itano, K.; Iizuka, T.; Hoshino, M. REE-Th-U and Nd isotope systematics of monazites in magnetite- and ilmenite-series granitic rocks of the Japan arc: Implications for its use as a tracer of magma evolution and detrital provenance. *Chem. Geol.* **2018**, *484*, 69–80. [CrossRef]
42. Kempe, U.; Lehmann, B.; Wolf, D.; Rodionov, N.; Bombach, K.; Schwengfelder, U.; Dietrich, A. U-Pb SHRIMP geochronology of Th-poor, hydrothermal monazite: An example from the Llallagua tin-porphyry deposit, Bolivia. *Geochim. Cosmochim. Acta* **2008**, *72*, 4352–4366. [CrossRef]
43. Boynton, W.V. *Cosmochemistry of the Rare Earth Elements*; Elsevier: Amsterdam, The Netherlands, 1984.
44. Bergemann, C.; Gnos, E.; Berger, A.; Whitehouse, M.; Mullis, J.; Wehrens, P.; Pettke, T.; Janots, E. Th-Pb ion probe dating of zoned hydrothermal monazite and its implications for repeated shear zone activity: An example from the Central Alps, Switzerland. *Tectonics* **2017**, *36*, 671–689. [CrossRef]
45. Hsü, K.J.; Li, J.L.; Chen, H.H.; Wang, Q.C.; Sun, S.; Şengör, A.M.C. Tectonics of South China: Key to understanding West Pacific geology. *Tectonophysics* **1990**, *183*, 9–39. [CrossRef]
46. Holloway, N.H. North Palawan block, Philippines—Its relation to Asian mainland and role in evolution of South China Sea. *Am. Assoc. Pet. Geol. Bull.* **1982**, *66*, 1355–1383. [CrossRef]
47. Ren, J.S. On the geotectonics of Southern China. *Acta Geol. Sin.* **1991**, *4*, 111–130.
48. Li, X.H.; Li, W.X.; Li, Z.X. On the genetic classification and tectonic implications of the Early Yanshanian granitoids in the Nanling Range, South China. *Chin. Sci. Bull.* **2007**, *52*, 1873–1885. [CrossRef]
49. Shu, L.S. An analysis of principal features of tectonic evolution in South China Block. *Geol. Bull. China* **2012**, *31*, 1035–1053, (In Chinese with English Abstract).
50. Charvet, J. The Neoproterozoic–Early Paleozoic tectonic evolution of the South China Block: An overview. *J. Asian Earth Sci.* **2013**, *74*, 198–209. [CrossRef]
51. Song, M.J.; Shu, L.S.; Santosh, M. Early Mesozoic intracontinental orogeny and stress transmission in South China: Evidence from Triassic peraluminous granites. *J. Geol. Soc.* **2017**, *174*, 591–607. [CrossRef]
52. Chen, P.R.; Kong, X.G.; Wang, Y.X.; Ni, Q.S.; Zhang, B.T.; Ling, H.F. Rb-Sr isotopic dating and significance of early Yanshanian bimodal volvanic-intrusive complex from South Jiangxi Province. *Geol. J. China Univ.* **1999**, *5*, 378–383, (In Chinese with English Abstract).
53. Fan, W.M.; Wang, Y.J.; Gao, F.; Peng, T.P. Mesozoic mafic magmatism in Hunan-Jiangxi Provinces and the lithospheric extension. *Earth Sci. Front. (China Univ. Geosci. Beijing)* **2003**, *10*, 159–169, (In Chinese with English Abstract).
54. Shu, L.S.; Faure, M.; Wang, B.; Zhou, X.M.; Song, B. Late Palaeozoic–Early Mesozoic geological features of South China: Response to the Indosinian collision events in Southeast Asia. *Comptes Rendus Geosci.* **2008**, *340*, 151–165. [CrossRef]
55. Zhang, G.W.; Guo, A.L.; Wang, Y.J.; Li, S.Z.; Dong, Y.P.; Liu, S.F.; He, D.F.; Cheng, S.Y.; Lu, R.K.; Yao, A.P. Tectonics of South China continent and its implications. *Sci. China Earth Sci.* **2013**, *56*, 1804–1828. (In Chinese) [CrossRef]
56. Shu, L.S.; Wang, B.; Cawood, P.A.; Santosh, M.; Xu, Z.Q. Early Paleozoic and Early Mesozoic intraplate tectonic and magmatic events in the Cathaysia Block, South China. *Tectonics* **2015**, *34*, 1600–1621. [CrossRef]
57. Xu, X.S.; Deng, P.; Reilly, S.Y.O.; Griffin, W.L.; Zhou, X.M.; Tan, Z.Z. Single zircon LA-ICP-MS U-Pb dating of Guidong complex (SE China) and its petrogenetic significance. *Chin. Sci. Bull.* **2003**, *48*, 1328–1334. (In Chinese) [CrossRef]
58. Liu, F.L.; Xu, Z.Q.; Liou, J.G.; Song, B. SHRIMP U-Pb ages of ultrahigh-pressure and retrograde metamorphism of gneisses, south-western Sulu terrane, eastern China. *J. Metamorph. Geol.* **2004**, *22*, 315–326. [CrossRef]
59. Li, X.H.; Li, Z.X.; Li, W.X.; Wang, Y.J. Initiation of the Indosinian Orogeny in South China: Evidence for a Permian Magmatic Arc on Hainan Island. *J. Geol.* **2006**, *114*, 341–353. [CrossRef]
60. Sun, T.; Zhou, X.M.; Chen, P.R.; Li, H.M.; Zhou, H.Y.; Wang, Z.C.; Shen, W.Z. The original model and tectonic setting for Mesozoic granites in Eastern Nanling Mountain Range. *Sci. China* **2003**, *33*, 1209–1218, (In Chinese with English Abstract).
61. Liu, F.L.; Xu, Z.Q.; Yang, J.S.; Zhang, Z.M.; Xu, H.M.; Li, T.F. Geochemical characteristics and UHP metamorphism of granitic gneisses in the main drilling hole of Chinese Continental Scientific Drilling Project and its adjacent area. *Acta Petrol. Sin.* **2004**, *20*, 9–26, (In Chinese with English Abstract).
62. Guo, C.L.; Zheng, J.H.; Lou, F.S.; Zeng, Z.L. Petrography, Genetic Types and Geological Dynamical Settings of the Indosinian Granitoids in South China. *Geotecton. Metallog.* **2012**, *36*, 457–472, (In Chinese with English Abstract).
63. Sylvester, P.J. Post-collisional strongly peraluminous granites. *Lithos* **1998**, *45*, 29–44. [CrossRef]

64. Potratz, G.L.; Geraldes, M.C.; Martins, M.V.A.; De Almeida, B.S. Sana Granite, a post-collisional S-type magmatic suite of the Ribeira Belt (Rio de Janeiro, SE Brazil). *Lithos* **2021**, *388–389*, 106077. [CrossRef]
65. Zhou, X.M.; Sun, T.; Shen, W.Z.; Niu, Y.L. Petrogenesis of Mesozoic granitoids and volcanic rocks in South China: A response to tectonic evolution. *Episodes* **2006**, *29*, 26–33. [CrossRef] [PubMed]
66. Mao, J.W.; Li, H.Y.; Hidehiko, S.; Louis, R.; Bernard, G. Geology and Metallogeny of the Shizhuyuan Skarn-Greisen Deposit, Hunan Province, China. *Int. Geol. Rev.* **1996**, *38*, 1020–1039.
67. Wang, F.Y.; Li, C.Y.; Ling, M.X.; Zhang, H.; Sun, Y.L.; Sun, W.D. Geochronology of the Xihuashan Tungsten Deposit in Southeastern China: Constraints from Re-Os and U-Pb Dating. *Resour. Geol.* **2011**, *61*, 414–423. [CrossRef]
68. Guo, C.L.; Chen, F.C.; Zeng, Z.L.; Lou, F.S. Petrogenesis of the Xihuashan granites in southeastern China: Constraints from geochemistry and in-situ analyses of zircon U-Pb-Hf-O isotopes. *Lithos* **2012**, *148*, 209–227. [CrossRef]
69. Shu, X.J.; Wang, X.L.; Sun, T.; Xu, X.S.; Dai, M.N. Trace elements, U-Pb ages and Hf isotopes of zircons from Mesozoic granites in the western Nanling Range, South China: Implications for petrogenesis and W-Sn mineralization. *Lithos* **2011**, *127*, 468–482. [CrossRef]
70. Xiong, Y.Q.; Shao, Y.J.; Cheng, Y.B.; Jiang, S.Y. Discrete Jurassic and Cretaceous Mineralization Events at the Xiangdong W(-Sn) Deposit, Nanling Range, South China. *Econ. Geol.* **2020**, *115*, 385–413. [CrossRef]
71. Zhang, J.; Liu, X.X.; Zeng, Z.L.; Li, W.; Peng, L.L.; Hu, H.B.; Cheng, J.W.; Lu, K.X. Age constraints on the genesis of the Changkeng tungsten deposit, Nanling region, South China. *Ore Geol. Rev.* **2021**, *134*, 104134. [CrossRef]
72. Liu, X.X.; Zhang, J.; Huang, F.; Cheng, J.W.; Lu, K.X.; Yang, J.F.; Wang, M.; Wang, Y.; Qiu, J.; Zhang, X. Tungsten deposits in southern Jiangxi Province: Constraints on the origin of wolframite from in-situ U-Pb isotope dating. *Ore Geol. Rev.* **2022**, *143*, 104774. [CrossRef]
73. Huang, J.Q.; Chen, T.Y. On the problem of polycyclic mineralization of tungsten and tnd deposits in South China. *Geol. Rev.* **1986**, *32*, 138–143, (In Chinese with English Abstract).
74. Zhang, W.L.; Hua, R.M.; Wang, R.C.; Chen, P.R.; Li, H.M. New Dating of the Dajishan Granite and Related Tungsten Mineralization in Southern Jiangxi. *Acta Geol. Sin.* **2006**, *80*, 956–962, (In Chinese with English Abstract).
75. Zhai, W.; Sun, X.M.; Wu, Y.S.; Sun, H.Y.; Hua, R.M.; Li, W.Q. 40Ar-39Ar dating of Yaoling tungsten deposit in northern Guangdong Province and SHRIMP U-Pb zircon age of related granites. *Miner. Depos.* **2011**, *30*, 21–32, (In Chinese with English Abstract).
76. Dou, H.R.; Zhang, W.L.; Wang, R.C.; Chen, W.D. Chronology, metallogenic fluid properties and evolution of the Niutangling tungsten deposit, Northern Guangxi, China. *Acta Geol. Sin.* **2018**, *92*, 2269–2300, (In Chinese with English Abstract).
77. Feng, C.Y.; Huang, F.; Qu, W.J.; Zeng, Z.L.; Ding, M. Molybdenite Re-Os Isotopic Dating on Diferent Types of Tungsten Deposits in Southeast of Jiulongnao Orefield and Its Geological Significances. *China Tungsten Ind.* **2011**, *26*, 6–11, (In Chinese with English Abstract).
78. Guo, C.L.; Lin, Z.Y.; Wang, D.H.; Chen, W.; Zhang, Y.; Feng, C.Y.; Chen, Z.H.; Zeng, Z.L.; Cai, R.Q. Petrologic Characteristics of the Granites and Greisens and Muscovite $^{40}Ar/^{39}Ar$ Dating in the Taoxikeng Tungsten Polymetallic Deposit, Southern Jiangxi Province. *Acta Geol. Sin.* **2008**, *82*, 1274–1284, (In Chinese with English Abstract).
79. Zhai, W.; Sun, X.M.; Wu, Y.S.; Sun, H.Y.; Hua, R.M.; Yang, Y.Q.; Li, S.H. Zircon SHRIMP U-Pb Dating of the Buried Granodiorite and Muscovite $^{40}Ar/^{39}Ar$ Dating of Mineralization and Geological Implications of Meiziwo Tungsten Deposit, Northern Guangdong Province, China. *Geol. J. China Univ.* **2010**, *16*, 177–185, (In Chinese with English Abstract).
80. Li, G.L.; Hua, R.M.; Wei, X.L.; Qu, W.J.; Huang, X.E.; Hu, D.Q.; Zhou, L.Q. Re-Os isotopic ages of two types of molybdenite from Zhangdongkeng tungsten deposit in Southern Jiangxi Province and their geologic implications. *Earth Sci.-J. China Univ. Geosci.* **2014**, *39*, 165–173, (In Chinese with English Abstract).
81. Feng, C.Y.; Zeng, Z.L.; Wang, S.; Liang, J.S.; Ding, M. SHRIMP Zircon U-Pb and Molybdenite Re-Os Dating of the Skarn-type Tungsten Deposits in Southern Jiangxi Province, China, and Geological Implications: Examplified by the Jiaoli and Baoshan Tungsten Polymetallic Deposits. *Geotecton. Et Metallog.* **2012**, *36*, 337–349, (In Chinese with English Abstract).
82. Cai, Y.; Ma, D.S.; Lu, J.J.; Huang, H.; Zhang, R.Q.; Qu, W.J. Re-Os geochronology and S isotope geochemistry of Dengfuxian tungsten deposit, Hunan Province, China. *Acta Petrol. Sin.* **2012**, *28*, 3798–3808, (In Chinese with English Abstract).
83. Lu, Y.Y.; Fu, J.M.; Li, C.B.; Cheng, S.B.; Chen, X.Q.; Ma, L.Y. Minerallization ages and prospecting significance for Qingshiling and Dalingbei tungsten deposits in Guidong-Rucheng area, Southern Hunan. *J. Guilin Univ. Technol.* **2018**, *38*, 14–23, (In Chinese with English Abstract).
84. Li, H.Q.; Liu, J.Q.; Du, G.M.; Wei, L. Geochronology of endogenetic metal deposits-Examplified by the Xihuashan Tungsten Deposit. *Chin. Sci. Bull.* **1992**, *38*, 1109–1112. (In Chinese)
85. Feng, C.Y.; Xu, J.X.; Zeng, Z.L.; Zhang, D.Q.; Qu, W.J.; She, H.Q.; Li, J.W.; Li, D.X.; Du, A.D.; Dong, Y.J. Zircon SHRIMP U-Pb and molybdenite Re-Os dating in Tianmenshan-Hongtaoling tungsten-tin orefield, Southern Jiangxi Province, China, and its geological implication. *Acta Geol. Sin.* **2007**, *81*, 952–963, (In Chinese with English Abstract).
86. Wang, Y.L.; Pei, R.F.; Li, J.W.; Wang, H.L.; Liu, X.F. Geochemical characteristics of granites from the Jiangjunzhai tungsten deposit of Southern Hunan Province and its Re-Os isotopic dating. *Rock Miner. Ana* **2009**, *28*, 274–278, (In Chinese with English Abstract).
87. Yin, Z.; Tao, J.L.; Li, H.W.; Gan, J.W.; Chen, W.; Li, X.W. Deposit geology, geochronology and metallogenic model of Helong W deposit in southern Jiangxi Province. *Acta Petrol. Sin.* **2021**, *37*, 1531–1552, (In Chinese with English Abstract).

88. Zhao, Z.; Chen, Y.C.; Zeng, Z.L.; Chen, Z.H.; Wang, D.H.; Zhao, B.; Zhang, J.J. Geological Characteristics and Petrogenic & Metallogenic Ages of the Yanqian Tungsten Deposit in Eastern Nanling Region. *J. Jilin Univ. (Earth Sci. Ed.)* **2013**, *43*, 1828–1839, (In Chinese with English Abstract).
89. Wang, X.F.; Qi, H.W.; Hu, R.Z.; Qu, W.J.; Peng, J.T.; Bi, X.W. Re-Os isotopic chronology of molybdenite from Hongling tungsten deposit of Guangdong Province and its geological significance. *Miner. Depos.* (In Chinese with English Abstract). **2010**, *29*, 415–426.
90. Wang, D.H.; Chen, Z.H.; Chen, Y.C.; Tang, J.X.; Li, J.K.; Ying, L.J.; Wang, C.H.; Liu, S.B.; Li, L.X.; Qin, Y.; et al. New data of the rock-forming and ore-forming chronology for China's important mineral resources areas. *Acta Petrol. Sin.* **2010**, *84*, 1030–1040, (In Chinese with English Abstract).
91. Li, W.S.; Ni, P.; Wang, G.G.; Yang, Y.L.; Pan, J.Y.; Wang, X.L.; Chen, L.L.; Fan, M.S. A possible linkage between highly fractionated granitoids and associated W-mineralization in the Mesozoic Yaogangxian granitic intrusion, Nanling region, South China. *J. Asian Earth Sci.* **2020**, *193*, 104314. [CrossRef]
92. Yang, B.; Zhao, L.; Chen, Z.L.; Mo, H.H.; Lu, J.; Tan, Y. U-Pb and Re-Os dating of the Jianlong Cu-W deposit in Xingguo County of southern Jiangxi Province: Constraint on its petrogenic and metallogenetic ages. *Geol. China* **2021**, *48*, 495–506, (In Chinese with English Abstract).
93. Wang, M.; Bai, X.J.; Yun, J.B.; Zhao, L.H.; Li, Y.L.; Wang, Z.Y.; Pu, Z.P.; Qiu, H.N. 40Ar-39Ar dating of mineralization of Shizhuyuan polymetallic deposit. *Geochemica* **2016**, *45*, 41–51, (In Chinese with English Abstract).
94. Fu, J.M.; Li, H.Q.; Qu, W.J.; Yang, X.J.; Wei, J.Q.; Liu, G.Q.; Ma, L.Y. Re-Os isotope dating of Da'ao tungsten-tin deposit in the Jiuyi Mountains, southern Hunan Province. *Geol. China* **2007**, *34*, 651–656, (In Chinese with English Abstract).
95. Yuan, S.D.; Zhang, D.L.; Shuang, Y.; Du, A.D.; Qu, W.J. Re-Os dating of molybdenite from the Xintianling giant tungsten-molybdenum deposit in southern Hunan Province, China and its geological implications. *Acta Petrol. Sin.* **2012**, *28*, 27–38, (In Chinese with English Abstract).
96. Wang, Y.L.; Chen, Y.C.; Wang, D.H.; Xu, J.; Chen, Z.H. Scheelite Sm-Nd dating of the Zhazixi W-Sb deposit in Hunan and its geological significance. *Geol. China* **2012**, *39*, 1339–1344, (In Chinese with English Abstract).
97. Liu, S.B.; Chen, Y.C.; Fan, S.X.; Xu, J.X.; Qu, W.J.; Yang, L.J. The second ore-prospecting space in the eastern and central parts of the Nanling metallogenic belt: Evidence from isotopic chronology. *Geol. China* **2010**, *37*, 1034–1049, (In Chinese with English Abstract).
98. Huang, F.; Feng, C.Y.; Chen, Y.C.; Ying, L.J.; Chen, Z.H.; Zeng, Z.L.; Qu, W.J. Isotopic Chronological Study of the Huangsha-Tieshanlong Quartz Vein-Type Tungsten Deposit and Timescale of Molybdenum Mineralization in Southern Jiangxi Province, China. *Acta Geol. Sin.* **2011**, *85*, 1434–1447.
99. Zhang, J.; Liu, X.X.; Li, W.; Zeng, Z.L.; Hu, H.B.; Peng, L.L.; Cheng, J.W.; Lu, K.X.; Li, P.Z. The metallogenic epoch and geological implications of the tungsten-tin polymetallic deposits in southern Jiangxi Province, China: Constraints from cassiterite U-Pb and molybdenite Re-Os isotopic dating. *Ore Geol. Rev.* **2021**, *134*, 104159. [CrossRef]